Molecules in Intense Laser Fields: Influence of the Nuclear Degrees of Freedom

Alejandro Saenz

AG Moderne Optik

Institut für Physik

Humboldt-Universität zu Berlin

(KITP Santa Barbara, 22.08.2014)

Acknowledgements: AMO group (June 2013)

Missing on the photo: Khaled Almhdi, Irina Dumitriu, Maike Ostmann, Stephen Okeyo, and Amon Kaufmann.

Acknowledgements:

Collaborators:

Piero Decleva (Trieste)
Alberto Castro (Zaragoza)
Erich Goll (Tübingen)
Günther Wunner (Stuttgart)

Ulrich Eichmann, Wolfgang Sandner (MBI)
Robert Moshammer, Joachim Ullrich (MPI)
Markus Gühr, Phil Bucksbaum (Stanford)

Financial support:

DFG

CORINF
Correlated Multielectron Dynamics in Intense Laser Fields

Bundesministerium für Bildung und Forschung

FCI
FONDS DER CHEMISCHEN INDUSTRIE

cost

DAAD
Deutscher Akademischer Austausch Dienst
German Academic Exchange Service
wandel durch austausch change by exchange

Stifterverband
für die Deutsche Wissenschaft

Overview

Introduction

Vibrational degrees of freedom:

- Dependence of the intense-field ionization yield on nuclear geometry.

Overview

Introduction

Vibrational degrees of freedom:

- Dependence of the intense-field ionization yield on nuclear geometry.
- Imaging nuclear motion:
  - ⋆ using the *Lochfraß* effect (total ion yield),

Overview

Introduction

Vibrational degrees of freedom:

- Dependence of the intense-field ionization yield on nuclear geometry.
- Imaging nuclear motion:
  - ⋆ using the *Lochfraß* effect (total ion yield),
  - ⋆ using PACER (high harmonics).

Overview

Introduction

Vibrational degrees of freedom:

- Dependence of the intense-field ionization yield on nuclear geometry.
- Imaging nuclear motion:
  - ⋆ using the *Lochfraß* effect (total ion yield),
  - ⋆ using PACER (high harmonics).
- Vibrational effects in low-intensity, high-frequency fields.

Overview

Introduction

Vibrational degrees of freedom:

- Dependence of the intense-field ionization yield on nuclear geometry.
- Imaging nuclear motion:
  - ⋆ using the *Lochfraß* effect (total ion yield),
  - ⋆ using PACER (high harmonics).
- Vibrational effects in low-intensity, high-frequency fields.

Rotational degrees of freedom:

- Alignment-dependent ionization in strong fields.

Overview

Introduction

Vibrational degrees of freedom:

- Dependence of the intense-field ionization yield on nuclear geometry.
- Imaging nuclear motion:
  - ⋆ using the *Lochfraß* effect (total ion yield),
  - ⋆ using PACER (high harmonics).
- Vibrational effects in low-intensity, high-frequency fields.

Rotational degrees of freedom:

- Alignment-dependent ionization in strong fields.
- Imaging electronic (orbital) densities.

Overview

Introduction

Vibrational degrees of freedom:

- Dependence of the intense-field ionization yield on nuclear geometry.
- Imaging nuclear motion:
  - ⋆ using the *Lochfraß* effect (total ion yield),
  - ⋆ using PACER (high harmonics).
- Vibrational effects in low-intensity, high-frequency fields.

Rotational degrees of freedom:

- Alignment-dependent ionization in strong fields.
- Imaging electronic (orbital) densities.

Summary

Motivation:

Understand the strong-field behaviour (ionization and excitation) of molecules in intense laser fields

Motivation:

Understand the strong-field behaviour (ionization and excitation) of molecules in intense laser fields

$\longrightarrow$ **relate molecular response to (instantaneous) molecular structure.**

Motivation:

Understand the strong-field behaviour (ionization and excitation) of molecules in intense laser fields

$\longrightarrow$ **relate molecular response to (instantaneous) molecular structure.**

Such relations would provide the basis for imaging!

Motivation:

Understand the strong-field behaviour (ionization and excitation) of molecules in intense laser fields

$\longrightarrow$ **relate molecular response to (instantaneous) molecular structure.**

Such relations would provide the basis for imaging!

Time-resolved imaging:

The advantage of strong-field imaging schemes would be the, in principle, possible time-resolution, e. g. by pump-probe experiments.

Motivation:

Understand the strong-field behaviour (ionization and excitation) of molecules in intense laser fields

$\longrightarrow$ relate molecular response to (instantaneous) molecular structure.

Such relations would provide the basis for imaging!

Time-resolved imaging:

The advantage of strong-field imaging schemes would be the, in principle, possible time-resolution, e. g. by pump-probe experiments.

Note, the original goal was to study "interesting", not (only) field-induced dynamics!

Chemical reaction mechanisms (I)

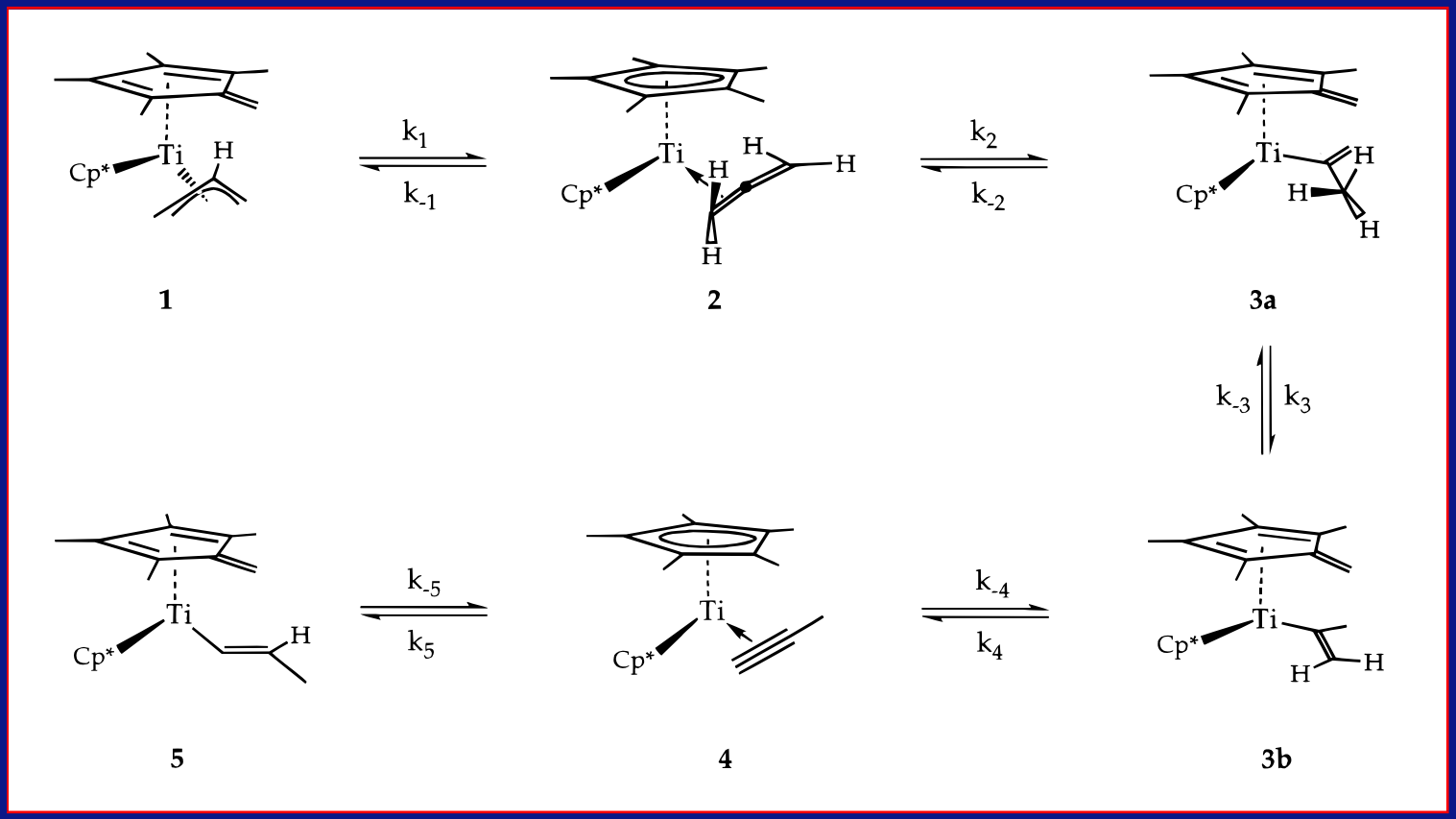

Determination of a reaction mechanism by following intermediates in time.

[Brinkmann, Luinstra, and A. S.; JACS **120** 2854 (1998).]

Chemical reaction mechanisms (II)

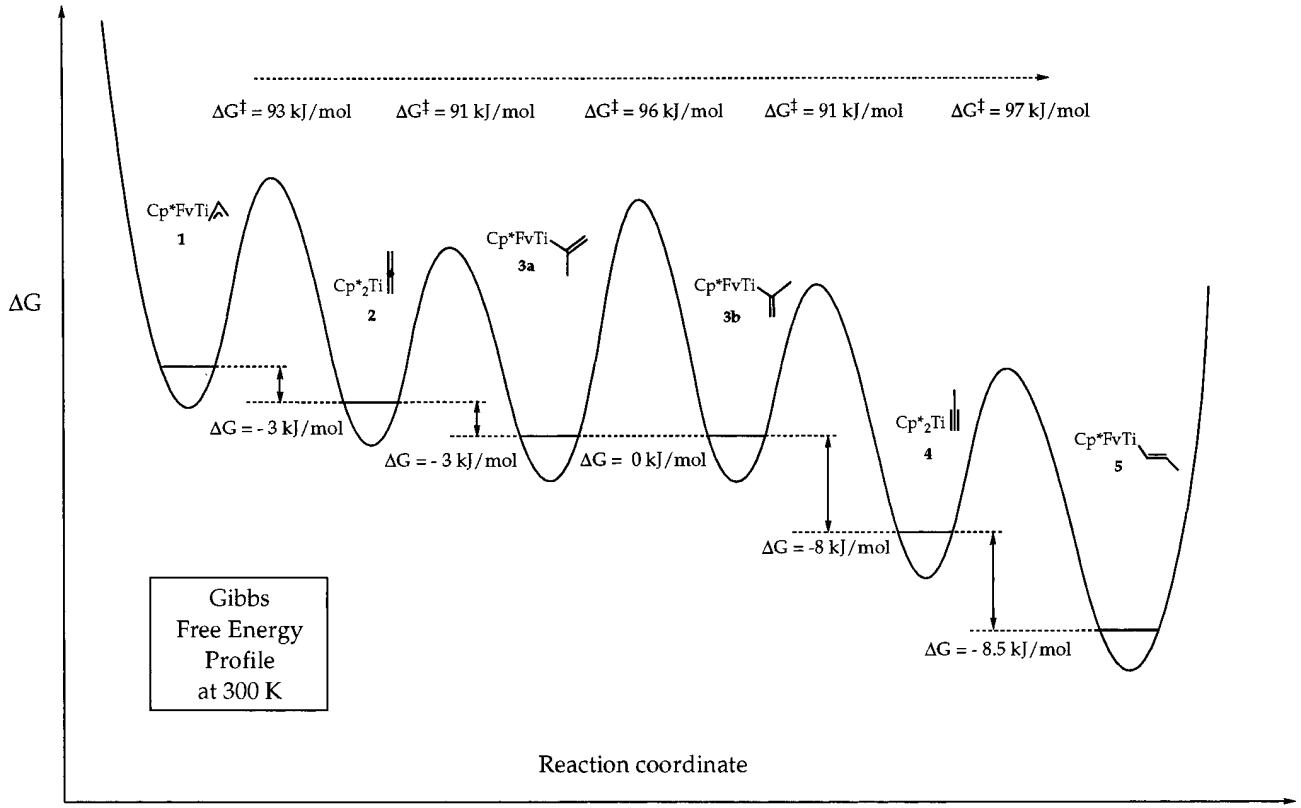

Figure 3. Gibbs free energy profile at 300 K for the isomerization of Cp*FvTi(allyl) (**1**) to Cp*FvTi-(*E*)-CH=CHMe (**5**).

Sequence of intermediates, kinetics and thermodynamics may (!) be disclosed.

However, the transition states remain invisible!

[Brinkmann, Luinstra, and A. S.; JACS **120** 2854 (1998).]

Corkum's 3-step model used for imaging

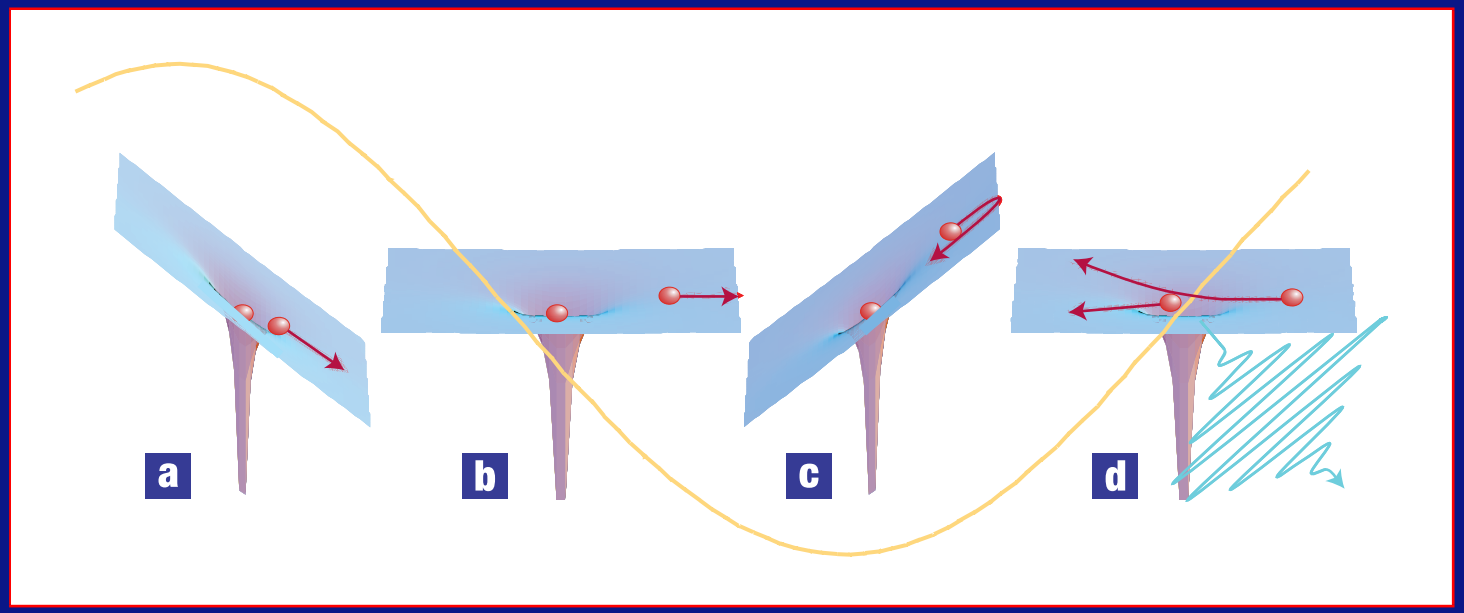

from P. B. Corkum and F. Krausz, *Nature Phys.* **3**, 381 (2007)

1. Electron escapes through or over the electric-field lowered Coulomb potential (a).
2. Electronic wavepacket moves away until the field direction reverses (b) and is (partly) driven back to its parent ion (c).
3. The returning electron may (d)
   - scatter elastically (electron diffraction)
   - scatter inelastically (excitation, dissociation, double ionization, . . .)
   - recombine radiatively (high-harmonic radiation).

Outcome of both the 1st and the 3rd step reveals time-resolved structure!

Proposed strong-field molecular imaging schemes:

Rescattering based (3rd step):

- orbital tomography using high harmonics [Nature **432**, 867 (2004)],
- PACER (nuclear geometry from high harmonics) [Science **312**, 424 (2006)],
- electron diffraction (using rescattered electrons) [Science **320**, 1478 (2008)].

Proposed strong-field molecular imaging schemes:

Rescattering based (3rd step):

- orbital tomography using high harmonics [Nature **432**, 867 (2004)],
- PACER (nuclear geometry from high harmonics) [Science **312**, 424 (2006)],
- electron diffraction (using rescattered electrons) [Science **320**, 1478 (2008)].

Direct-ionization based (1st step):

- "Lochfraß" (nuclear motion from ions or electrons) [PRL **97**, 103003 (2006)],
- alignment-dependent ionization (orbital shapes) [PRL **98**, 243001 (2007)],
- nuclear motion from energy-resolved e^- spectra [PRA **82**, 011403(R) (2010)].

Proposed strong-field molecular imaging schemes:

Rescattering based (3rd step):

- orbital tomography using high harmonics [Nature **432**, 867 (2004)],
- PACER (nuclear geometry from high harmonics) [Science **312**, 424 (2006)],
- electron diffraction (using rescattered electrons) [Science **320**, 1478 (2008)].

Direct-ionization based (1st step):

- "Lochfraß" (nuclear motion from ions or electrons) [PRL **97**, 103003 (2006)],
- alignment-dependent ionization (orbital shapes) [PRL **98**, 243001 (2007)],
- nuclear motion from energy-resolved e^- spectra [PRA **82**, 011403(R) (2010)].

Advantages of direct-ionization-based imaging:

- It delivers the image directly!

Proposed strong-field molecular imaging schemes:

Rescattering based (3rd step):

- orbital tomography using high harmonics [Nature **432**, 867 (2004)],
- PACER (nuclear geometry from high harmonics) [Science **312**, 424 (2006)],
- electron diffraction (using rescattered electrons) [Science **320**, 1478 (2008)].

Direct-ionization based (1st step):

- "Lochfraß" (nuclear motion from ions or electrons) [PRL **97**, 103003 (2006)],
- alignment-dependent ionization (orbital shapes) [PRL **98**, 243001 (2007)],
- nuclear motion from energy-resolved e^- spectra [PRA **82**, 011403(R) (2010)].

Advantages of direct-ionization-based imaging:

- It delivers the image directly!
- It is the by far dominating process!

Example electron spectrum (ATI)

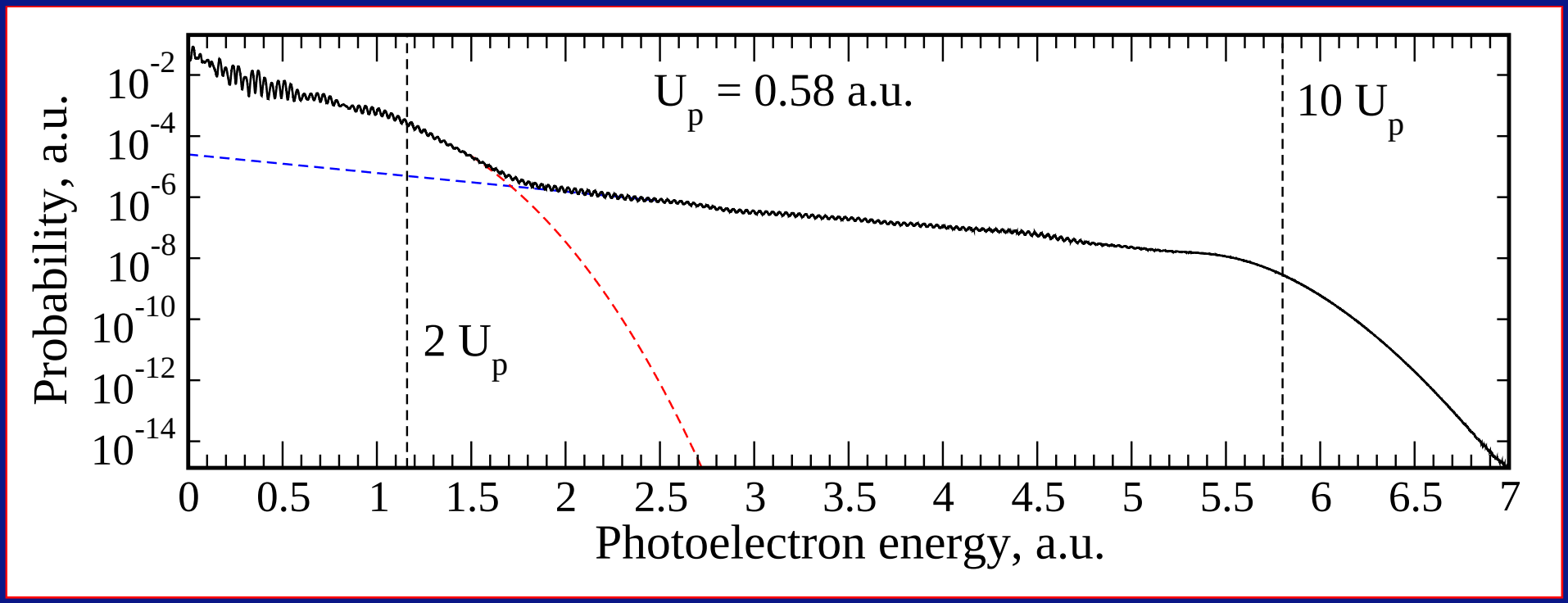

Technical details of the TDSE calculation:

Hydrogen atom

Laser parameters: 1300 nm; 6 cycles; $\cos^2$; $I_{\max} = 10^{14}\,\mathrm{W/cm^2}$.

Direct electrons: 0 to about 2 times the ponderomotive energy $\mathrm{U_p} = I/(4\omega^2)$.

Approximate models: tunneling ionization

Direct ionization for imaging: tunneling regime (low frequency, high intensity).

Approximate models: tunneling ionization

Direct ionization for imaging: tunneling regime (low frequency, high intensity).

Tunneling ionization (e. g., Ammosov-Delone-Krainov (ADK) model):

$$\Gamma_{\mathrm{ADK}}(F) \propto \exp\left[-\frac{2\,(2\,E_b)^{3/2}}{3F}\right]$$

with field strength F and electron's binding energy E_b.

Approximate models: tunneling ionization

Direct ionization for imaging: tunneling regime (low frequency, high intensity).

Tunneling ionization (e. g., Ammosov-Delone-Krainov (ADK) model):

$$\Gamma_{\mathrm{ADK}}(F) \propto \exp\left[-\frac{2\,(2\,E_b)^{3/2}}{3F}\right]$$

with field strength F and electron's binding energy E_b.

Advantage: Ionization at field maxima $\longrightarrow$ sub-lasercycle time resolution!

Approximate models: tunneling ionization

Direct ionization for imaging: tunneling regime (low frequency, high intensity).

Tunneling ionization (e. g., Ammosov-Delone-Krainov (ADK) model):

$$\Gamma_{\mathrm{ADK}}(F) \propto \exp\left[-\frac{2\,(2\,E_b)^{3/2}}{3F}\right]$$

with field strength F and electron's binding energy E_b.

Advantage: Ionization at field maxima $\longrightarrow$ sub-lasercycle time resolution!

Molecules: Nuclear-geometry dependence of tunnel ionization?

Molecular effects: R-dependence (extnd. ADK/SFA/. . . model)

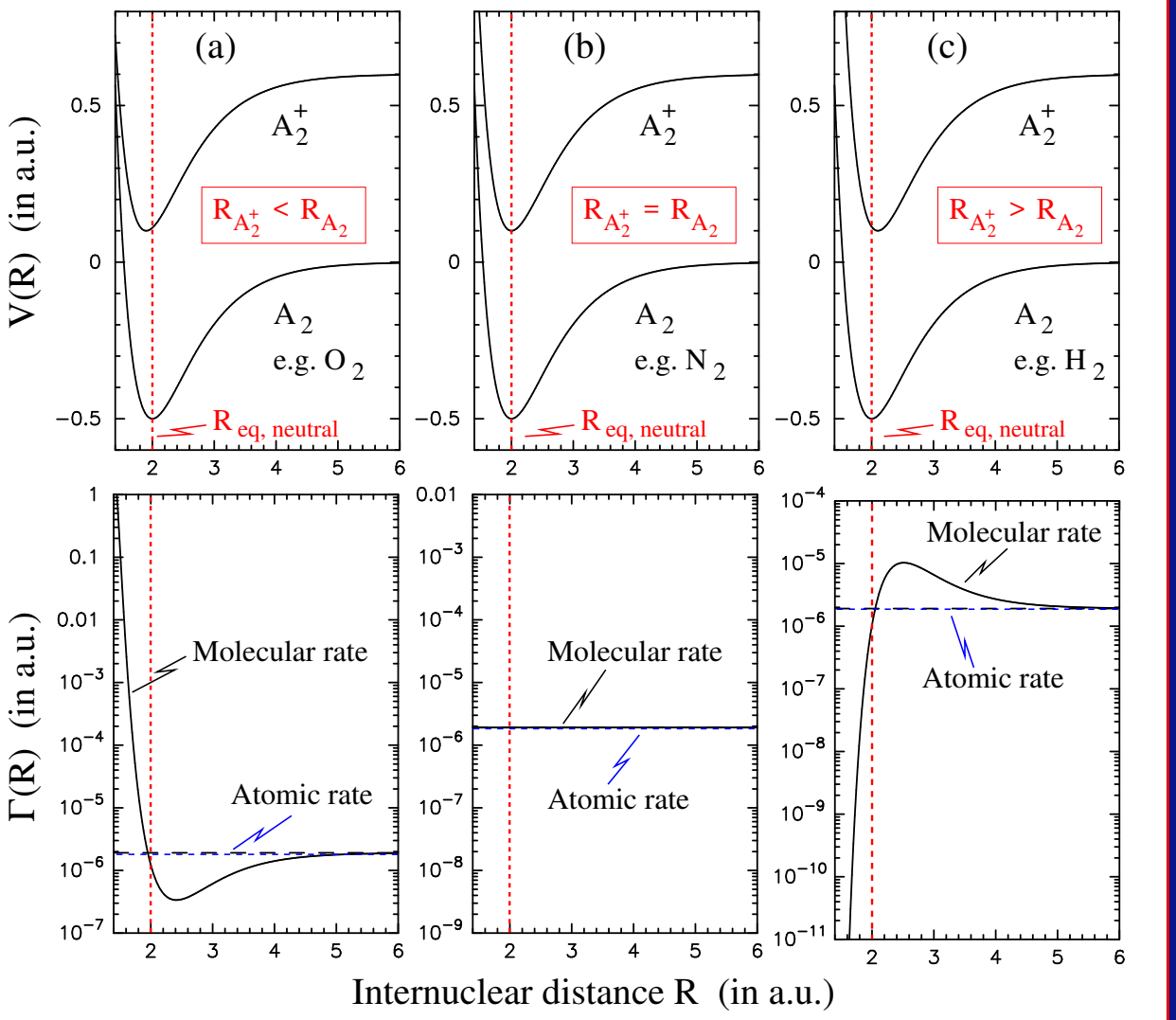

ADK model:

$$\Gamma_{\mathrm{ADK}} \propto \exp\left(-\frac{2\,(2\,I_P)^{3/2}}{3\,F}\right)$$

with

Γ_{ADK}: ionization rate

F: field strength

I_P: ionization potential

Extended ADK model:

Replace ionization potential I_P with $E^{\mathrm{A}_2^+}(R) - E^{\mathrm{A}_2}(R)$

No Franck-Condon distribution for, e. g., H_2 or O_2 [A.S., *J. Phys. B* **33**, 4365 (2000)].

R-dependent ab initio dc ionization rate for H_2

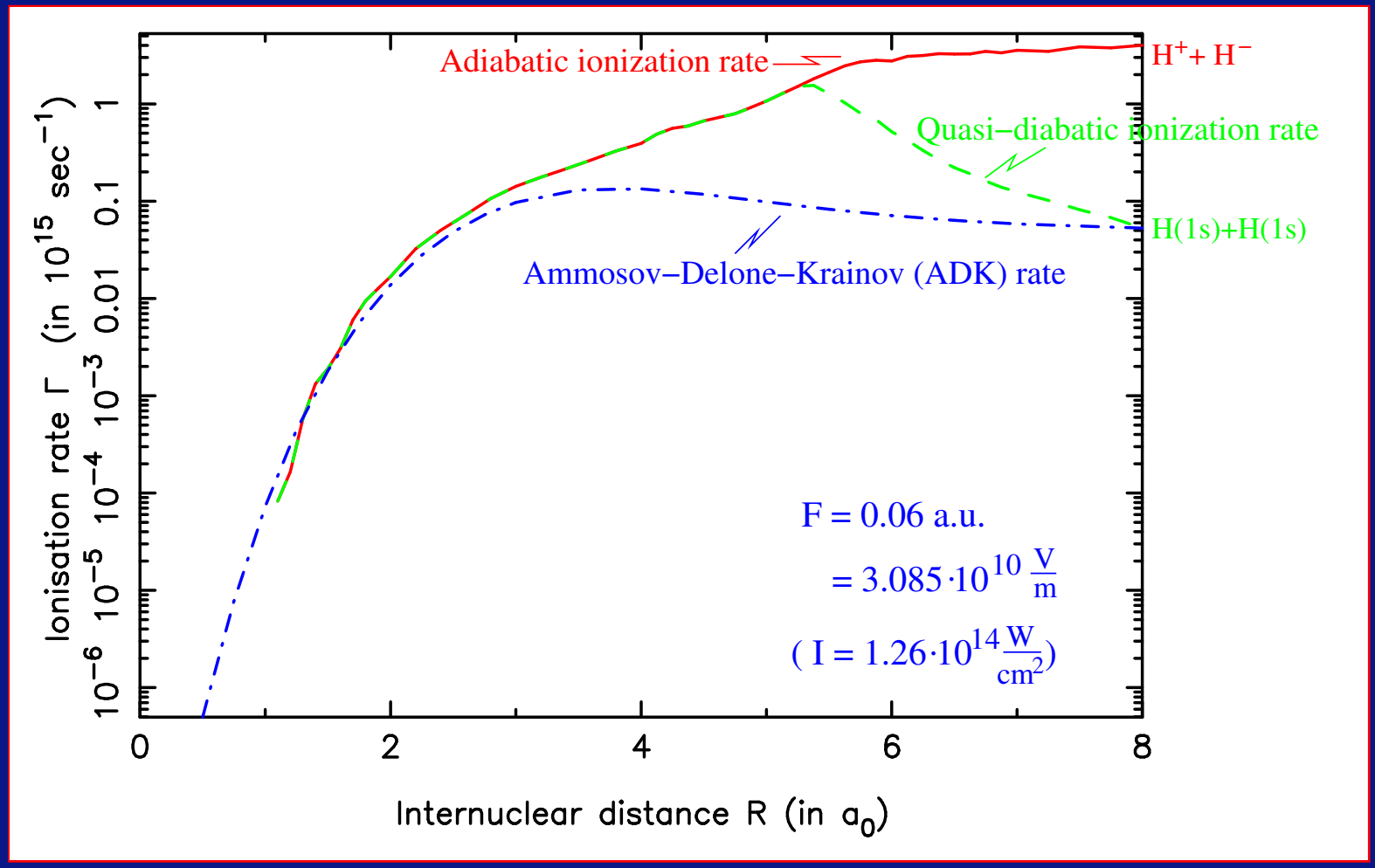

Ab initio calculation (dc field) confirms: ionisation rate of H_2 strongly R dependent.

[A.S., *Phys. Rev. A* **61**, 051402 (R) (2000); *Phys. Rev. A* **66**, 063408 (2002).]

H_2^+ vibrational distribution (theory vs. experiment)

$3.5 \cdot 10^{13} \frac{\mathrm{W}}{\mathrm{cm}^2}$

$5.4 \cdot 10^{13} \frac{\mathrm{W}}{\mathrm{cm}^2}$

$7.8 \cdot 10^{13} \frac{\mathrm{W}}{\mathrm{cm}^2}$

$1.1 \cdot 10^{14} \frac{\mathrm{W}}{\mathrm{cm}^2}$

Theory

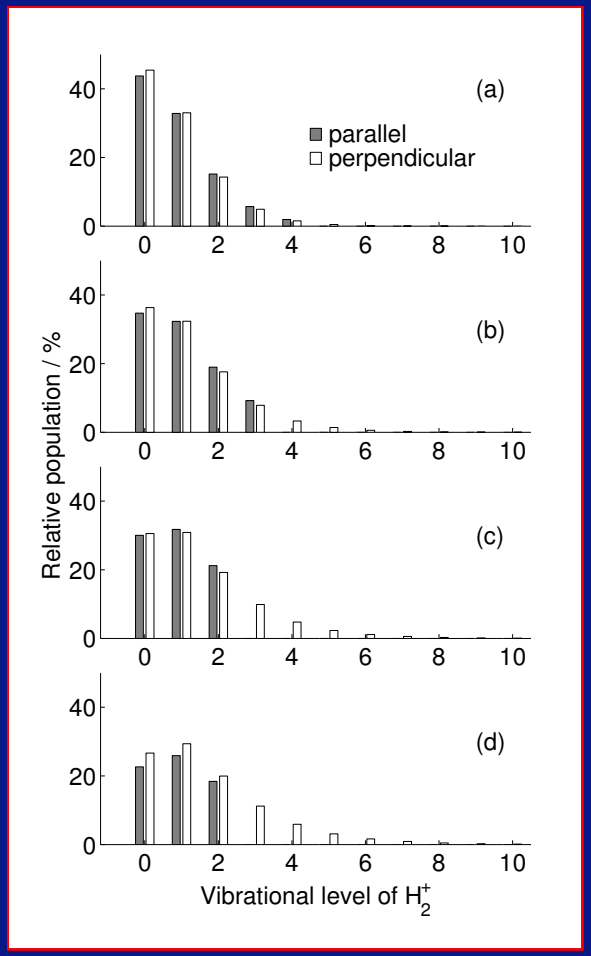

H_2^+ vibrational distribution (theory vs. experiment)

$3.5 \cdot 10^{13} \frac{\mathrm{W}}{\mathrm{cm}^2}$

$5.4 \cdot 10^{13} \frac{\mathrm{W}}{\mathrm{cm}^2}$

$7.8 \cdot 10^{13} \frac{\mathrm{W}}{\mathrm{cm}^2}$

$1.1 \cdot 10^{14} \frac{\mathrm{W}}{\mathrm{cm}^2}$

Theory

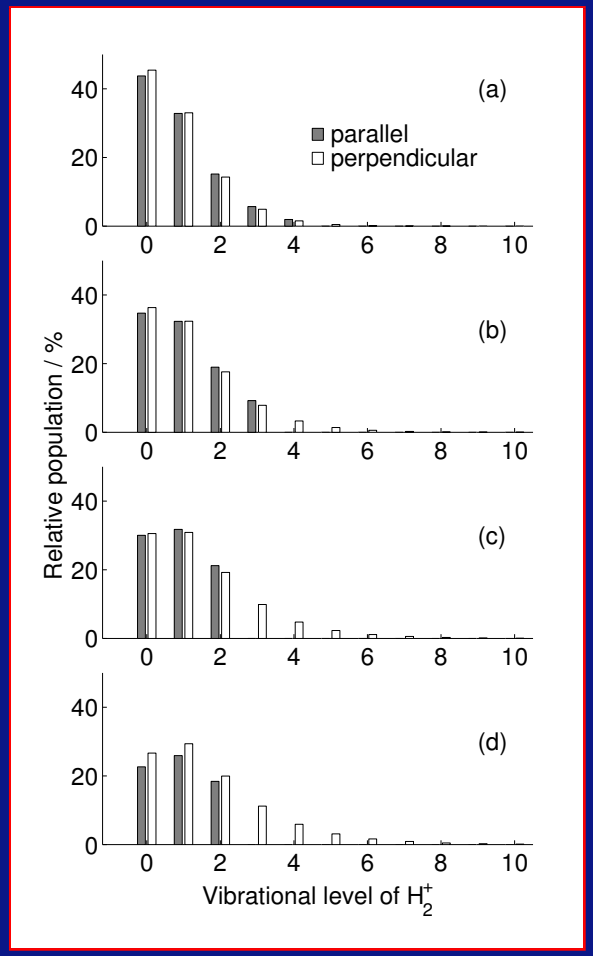

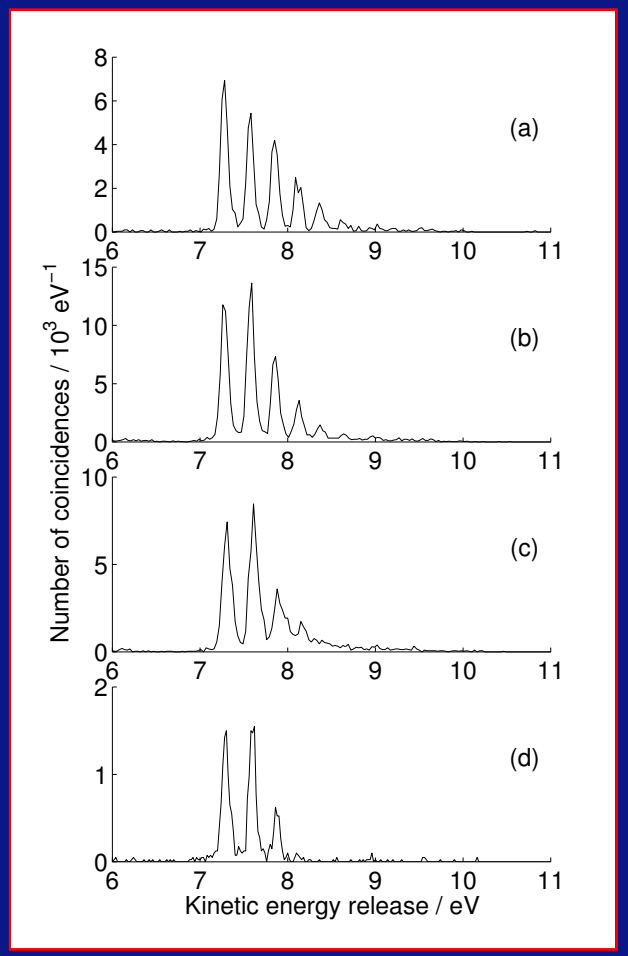

$3 \cdot 10^{13} \frac{\mathrm{W}}{\mathrm{cm}^2}$

$4.8 \cdot 10^{13} \frac{\mathrm{W}}{\mathrm{cm}^2}$

$1.5 \cdot 10^{14} \frac{\mathrm{W}}{\mathrm{cm}^2}$

$1 \cdot 10^{14} \frac{\mathrm{W}}{\mathrm{cm}^2}$
(ns-Laser)

Experiment

1. Only detection of undissociated H_2^+ ions.
2. Alignment of H_2 is pulse-length dependent.

Theory and experiment:

X. Urbain, . . . , A.S. *et al.*, *Phys. Rev. Lett.* **92**, 163004 (2004).

Validity of quasi-static approximation for H_2

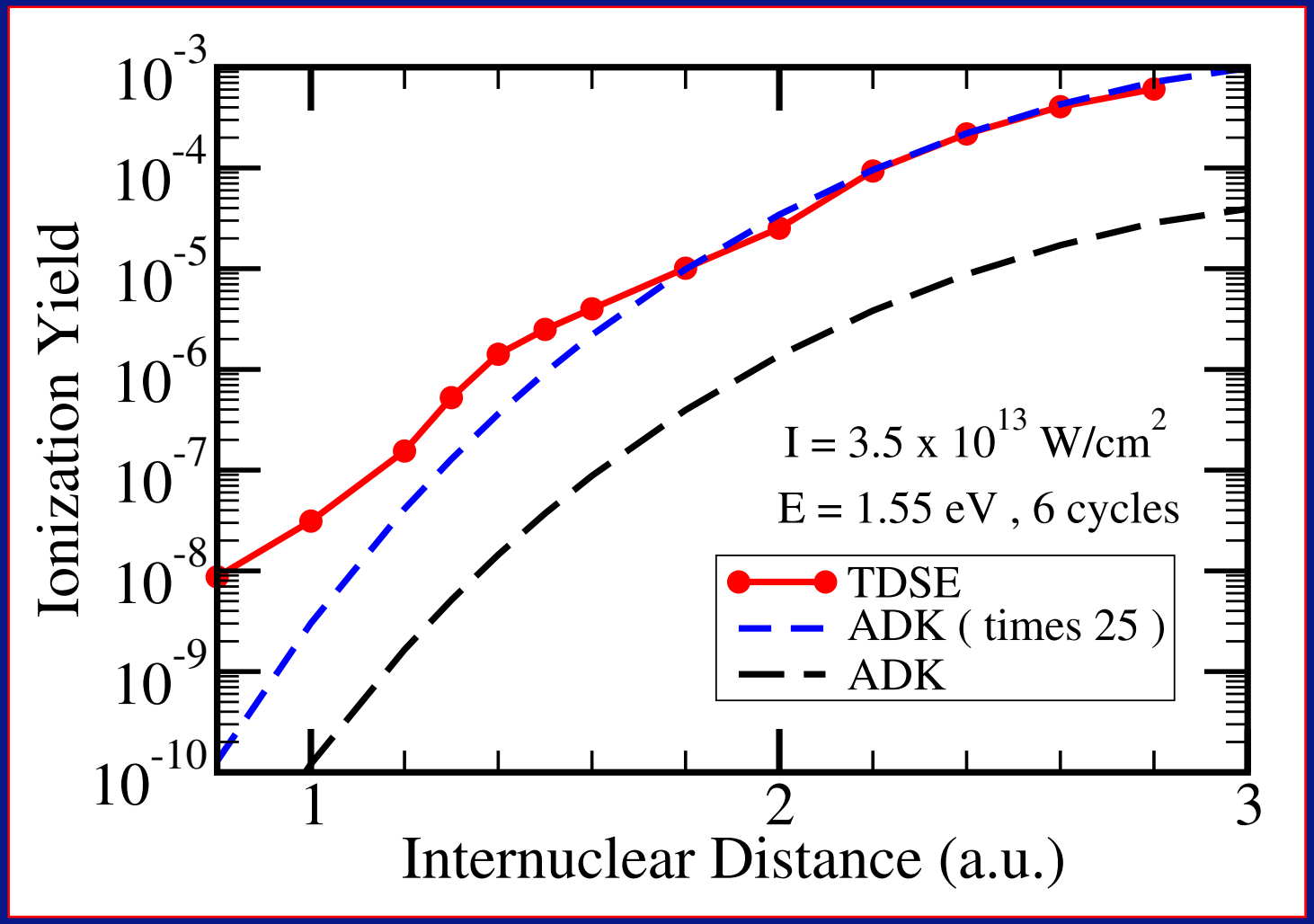

Full-dimensional solution of TDSE: M. Awasthi, Y. V. Vanne, A.S., *J. Phys. B* **38**, 3973 (2005) [method];
M. Awasthi and A.S., *J. Phys. B:* **39**, S389 (2006) [R dependence].

Frequency-corrected ADK (I)

- For 800 nm pulses with intensities between $I = 2 \cdot 10^{13} - 1.3 \cdot 10^{14}$ W/cm^2:

  Keldysh parameter $\gamma = \omega \frac{\sqrt{2I_p}}{F}$ varies between $\gamma = 0.67$ and 2.6

  $\rightarrow$ transition regime between the multiphoton and the quasi-static regime.

Frequency-corrected ADK (I)

- For 800 nm pulses with intensities between $I = 2 \cdot 10^{13} - 1.3 \cdot 10^{14}$ W/cm^2:

  Keldysh parameter $\gamma = \omega \frac{\sqrt{2I_p}}{F}$ varies between $\gamma = 0.67$ and 2.6

  $\rightarrow$ transition regime between the multiphoton and the quasi-static regime.

- Comparison to yields obtained from tunneling rates using
  $Y_{\mathrm{ADK}}(R) = 1 - \exp\left\{-\int \Gamma_{\mathrm{ADK}}[F(t), I_p(R)]dt\right\}$.

Frequency-corrected ADK (I)

- For 800 nm pulses with intensities between $I = 2 \cdot 10^{13} - 1.3 \cdot 10^{14}$ W/cm^2:

  Keldysh parameter $\gamma = \omega \frac{\sqrt{2I_p}}{F}$ varies between $\gamma = 0.67$ and 2.6

  $\rightarrow$ transition regime between the multiphoton and the quasi-static regime.

- Comparison to yields obtained from tunneling rates using $Y_{\mathrm{ADK}}(R) = 1 - \exp\left\{-\int \Gamma_{\mathrm{ADK}}[F(t), I_p(R)]dt\right\}$.

- Validity condition $\gamma \ll 1$ for ADK not strictly fulfilled.

Frequency-corrected ADK (I)

- For 800 nm pulses with intensities between $I = 2 \cdot 10^{13} - 1.3 \cdot 10^{14}$ W/cm^2:

  Keldysh parameter $\gamma = \omega\frac{\sqrt{2I_p}}{F}$ varies between $\gamma = 0.67$ and 2.6

  $\rightarrow$ transition regime between the multiphoton and the quasi-static regime.

- Comparison to yields obtained from tunneling rates using $Y_{\mathrm{ADK}}(R) = 1 - \exp\left\{-\int \Gamma_{\mathrm{ADK}}[F(t), I_p(R)]dt\right\}$.

- Validity condition $\gamma \ll 1$ for ADK not strictly fulfilled.

- **FC-ADK:** frequency-corrected ADK based on PPT

$$\Gamma_{\mathrm{FC-ADK}} = \Gamma_{\mathrm{ADK}} \times \exp\left[-\frac{2\kappa^3}{3F}\, g(\gamma)\right] / \exp\left[-\frac{2\kappa^3}{3F}\right]$$

$$g(\gamma) = \frac{3}{2\gamma}\left\{\left(1 + \frac{1}{2\gamma^2}\right)\mathrm{arcsinh}\gamma - \frac{\sqrt{1+\gamma^2}}{2\gamma}\right\}$$

Frequency-corrected ADK (II)

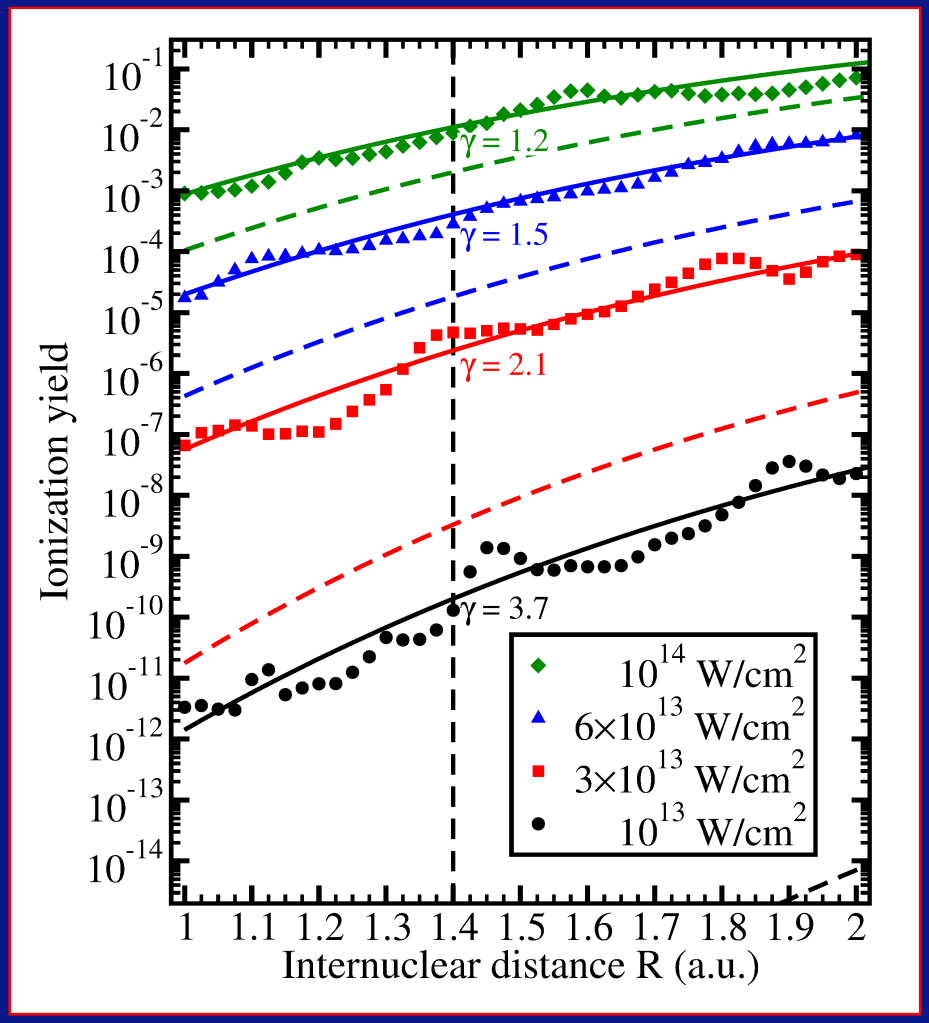

TDSE (points) vs. ADK (dashed lines) and FC-ADK (full lines)

(Laser parameters: 40-cycle $\cos^2$, 800 nm.)

Incorporation of nuclear motion

Different levels of approximation:

FNA: fixed-nuclei approximation, ion yield/rate $Y_{\mathrm{FNA}} = Y(\vec{R}_{\mathrm{eq}})$ with equilibrium geometry vectors $\vec{R}_{\mathrm{eq}}$

$\longrightarrow$ complete neglect of vibrational motion.

Incorporation of nuclear motion

Different levels of approximation:

FNA: fixed-nuclei approximation, ion yield/rate $Y_{\mathrm{FNA}} = Y(\vec{R}_{\mathrm{eq}})$ with equilibrium geometry vectors $\vec{R}_{\mathrm{eq}}$

$\longrightarrow$ complete neglect of vibrational motion.

FROZ: frozen-nuclei approximation, ion yield/rate $Y_{\mathrm{FROZ}} = \int Y(\vec{R}\,)\,|\chi(\vec{R}\,)|^2\,\mathrm{d}V_R$ with initial-state vibrational wavefunction $\chi(\vec{R}\,)$

$\longrightarrow$ considers initial (quantum) spread of nuclear wavefunction, but no nuclear dynamics initiated by the laser pulse.

Incorporation of nuclear motion

Different levels of approximation:

FNA: fixed-nuclei approximation, ion yield/rate $Y_{\mathrm{FNA}} = Y(\vec{R}_{\mathrm{eq}})$ with equilibrium geometry vectors $\vec{R}_{\mathrm{eq}}$

$\longrightarrow$ complete neglect of vibrational motion.

FROZ: frozen-nuclei approximation, ion yield/rate $Y_{\mathrm{FROZ}} = \int Y(\vec{R}\,)\,|\chi(\vec{R}\,)|^2\,\mathrm{d}V_R$ with initial-state vibrational wavefunction $\chi(\vec{R}\,)$

$\longrightarrow$ considers initial (quantum) spread of nuclear wavefunction, but no nuclear dynamics initiated by the laser pulse.

FULL: full inclusion of nuclear dynamics in the TDSE solution.

Incorporation of nuclear motion: example H_2

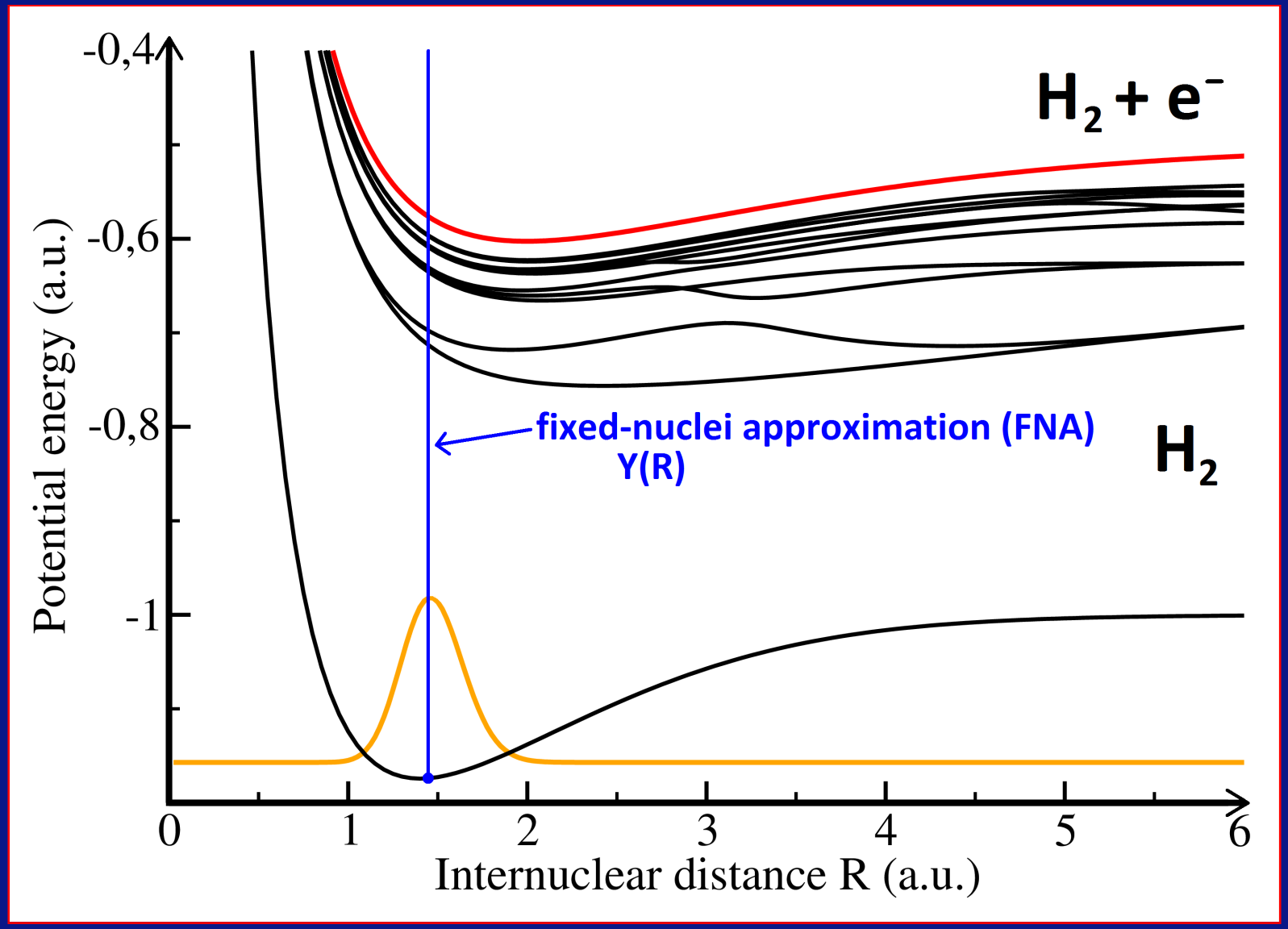

Incorporation of nuclear motion: example H_2

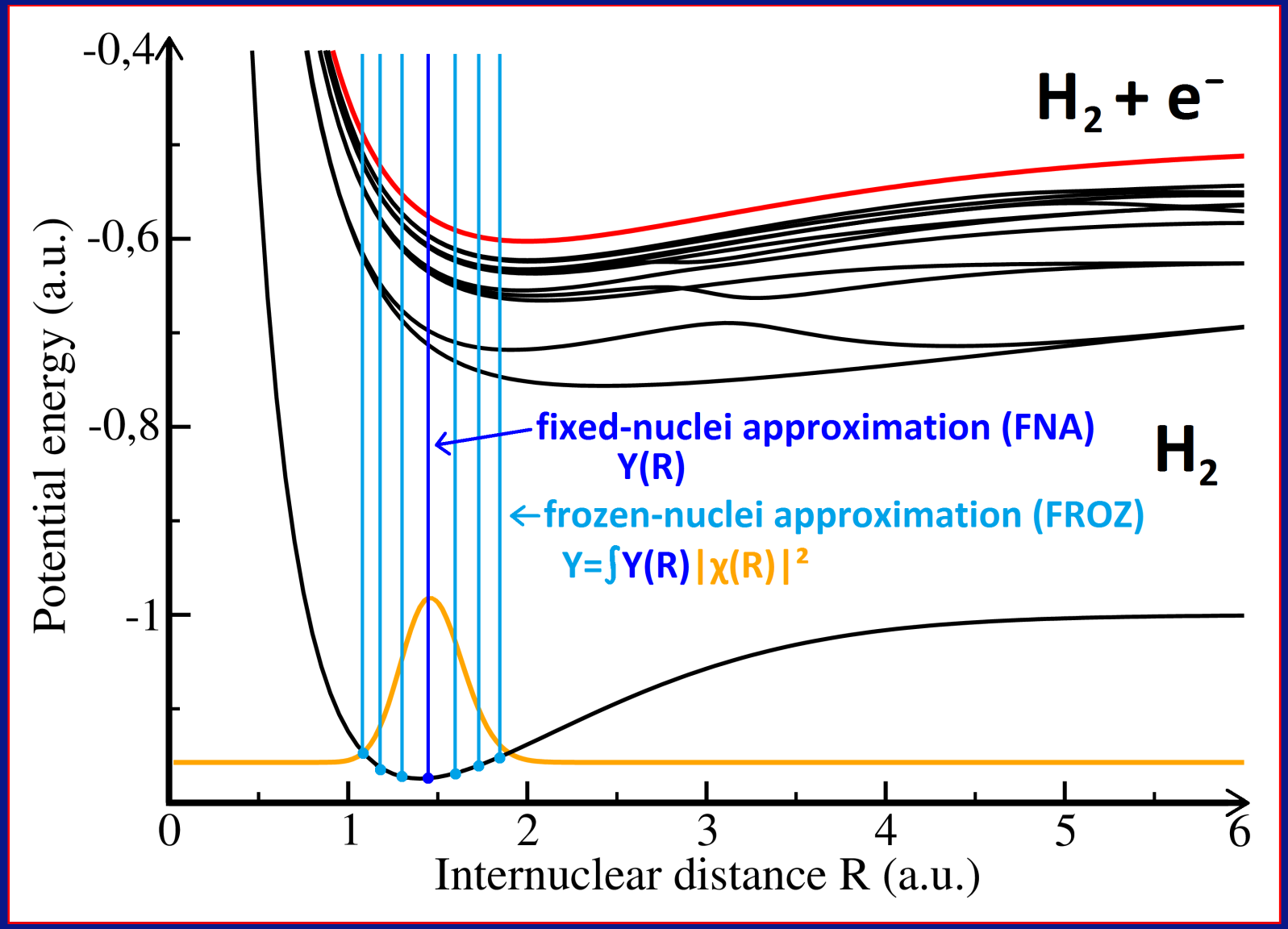

Incorporation of nuclear motion: example H_2

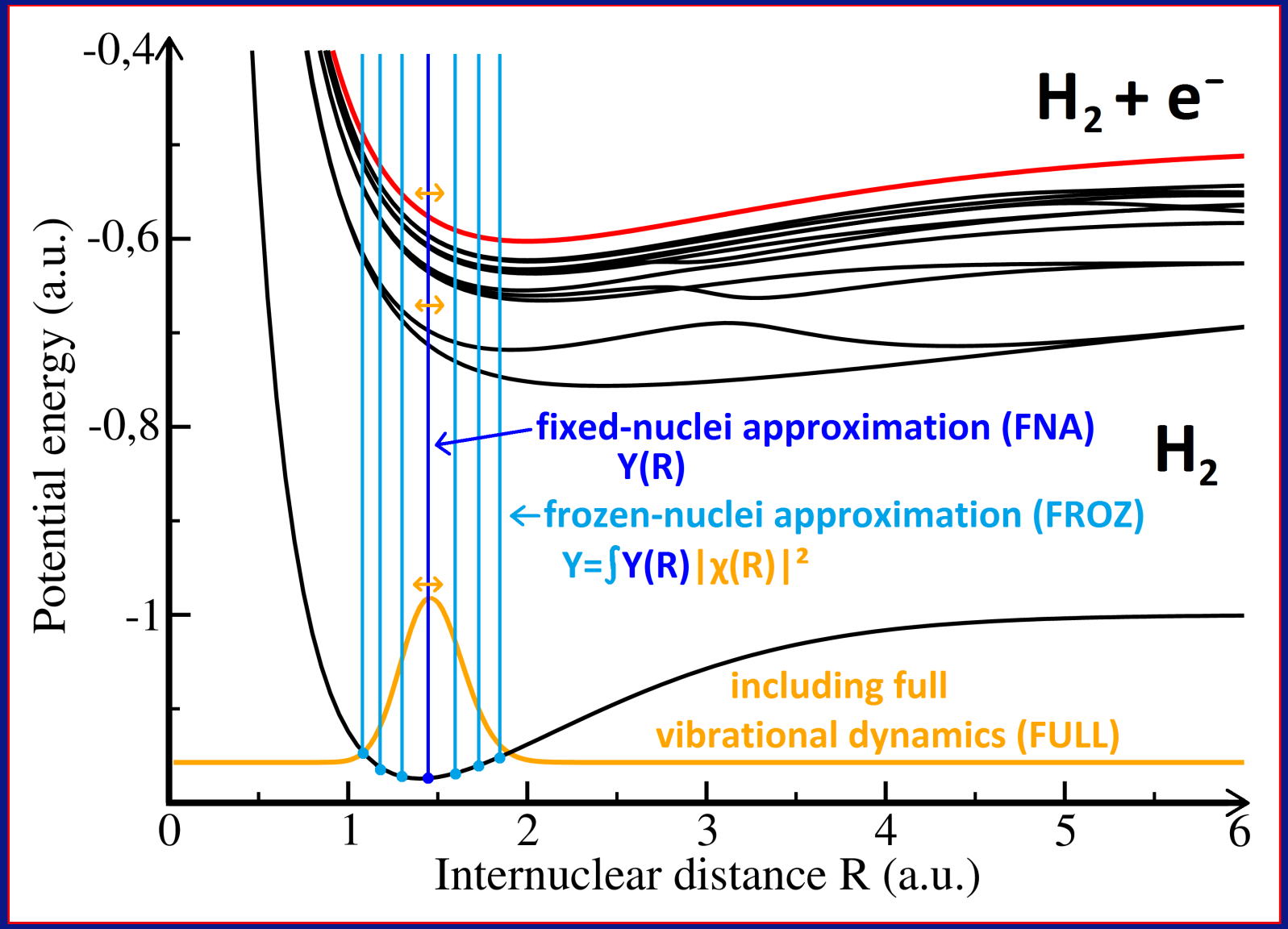

Nuclear motion in H_2 (800 nm, 20 cycles, parallel)

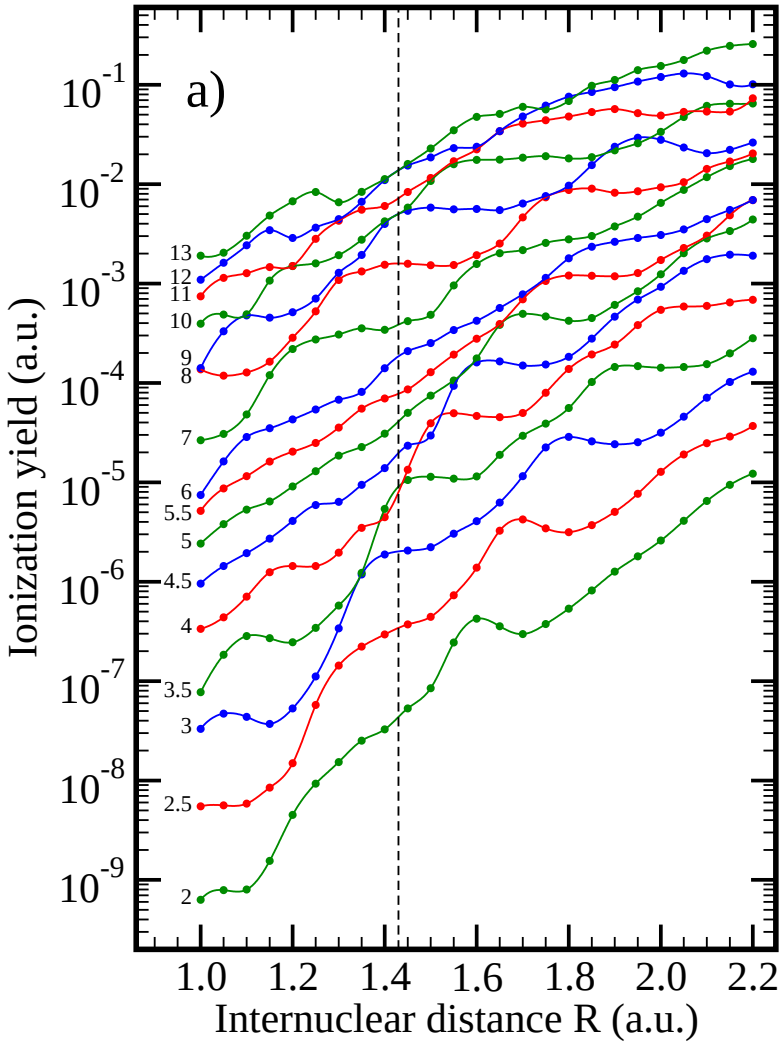

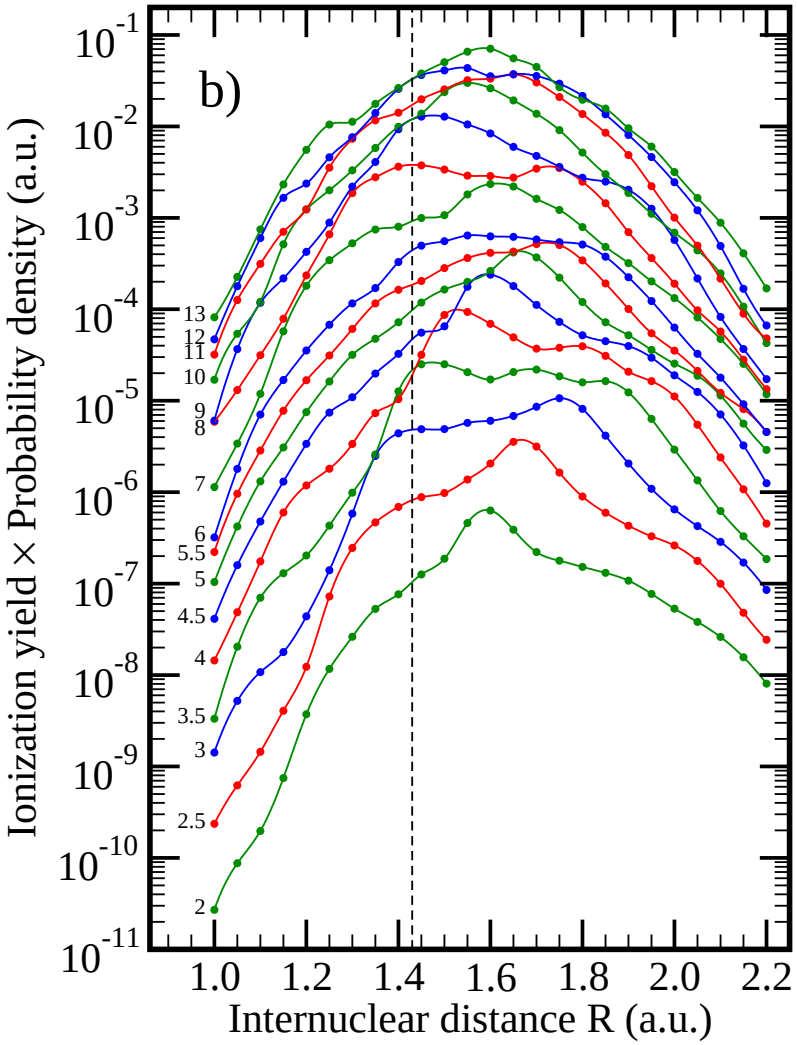

Yield for fixed R

Yield weighted with $|\Psi_{v=0}(R)|^2$

Nuclear motion in H_2 (800 nm, 20 cycles, perpendicular)

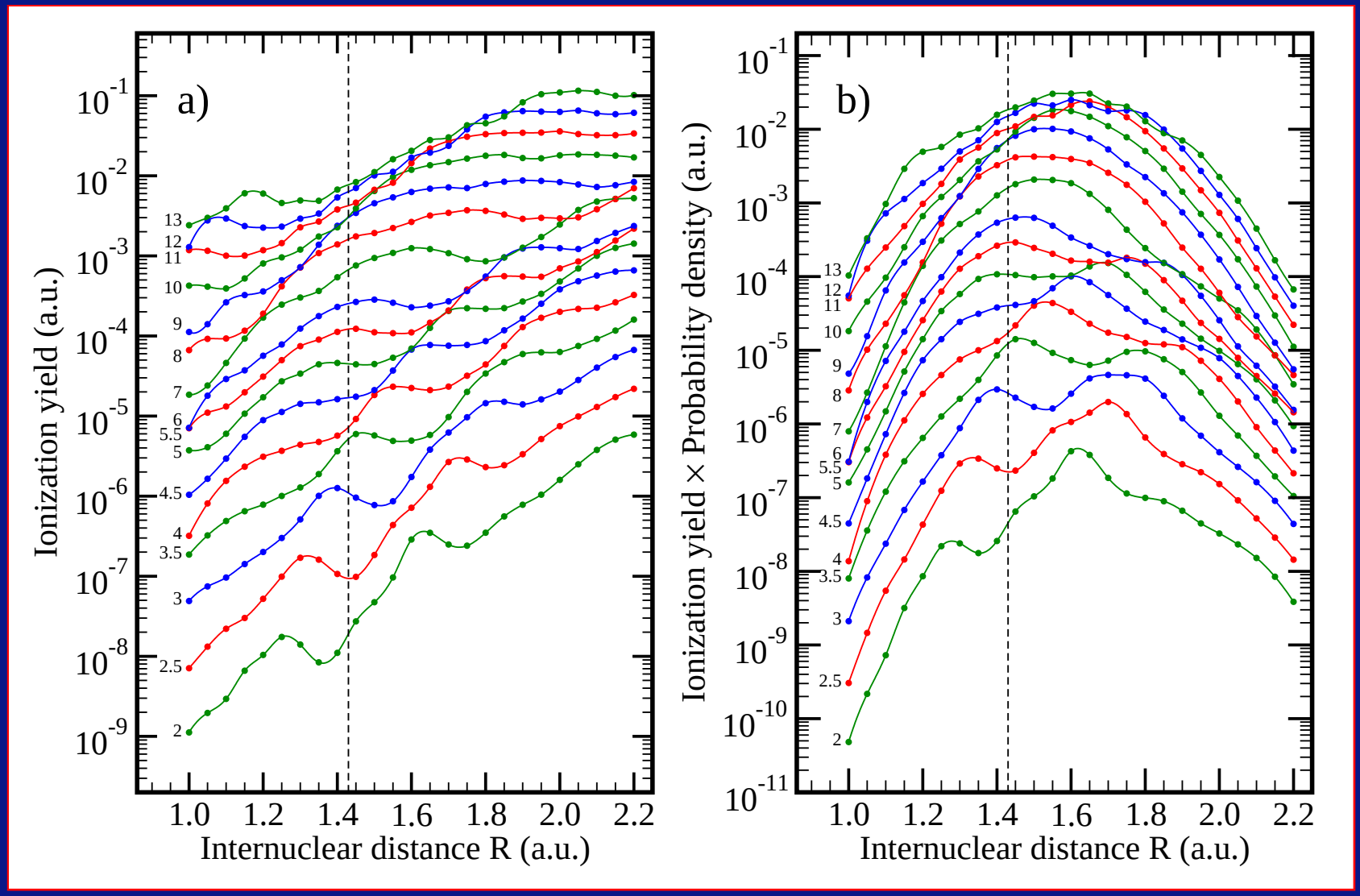

Yield for fixed R

Yield weighted with $|\Psi_{v=0}(R)|^2$

Comparison TDSE vs. ADK and fc-ADK (H_2, 800nm, 20 cycles)

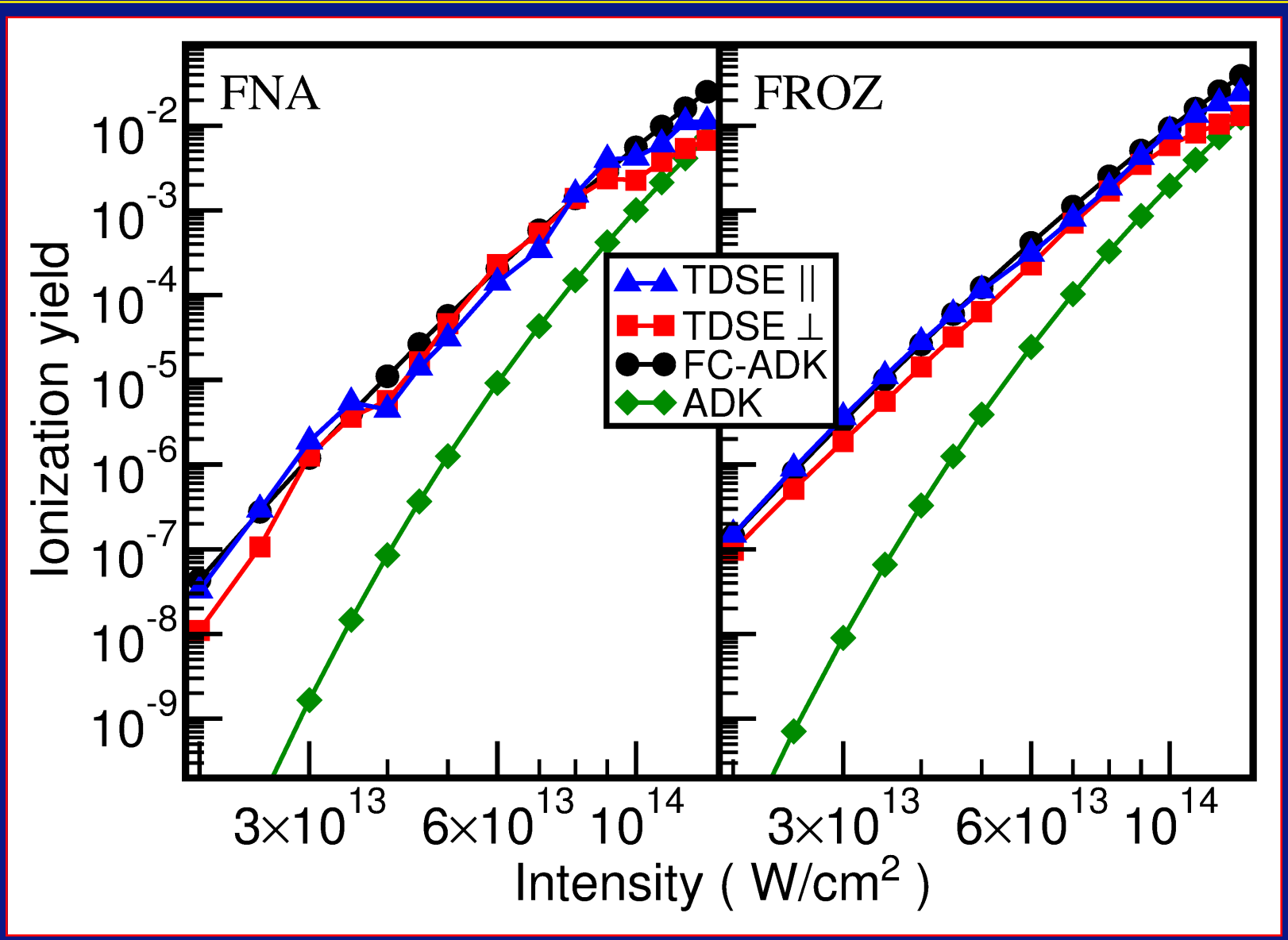

Ion yields in fixed (FNA, left) and frozen (FROZ, right) nuclei approximation.

Strong-Field Control: "Lochfrass" (Proposal)

- **Pronounced R-dependent ionization yield**

  $\longrightarrow$ **fast** ionization process (pump) should **deplete** the large R component of the wavefunction.

Strong-Field Control: "Lochfrass" (Proposal)

- **Pronounced R-dependent ionization yield**
  $\longrightarrow$ **fast** ionization process (pump) should **deplete** the large R component of the wavefunction.

- A coherent vibrational wavepacket in the electronic ground state of the **neutral(!)** molecule is created.

Strong-Field Control: "Lochfrass" (Proposal)

- **Pronounced R-dependent ionization yield**

  $\longrightarrow$ **fast** ionization process (pump) should **deplete** the large R component of the wavefunction.

- A coherent vibrational wavepacket in the electronic ground state of the **neutral(!)** molecule is created.

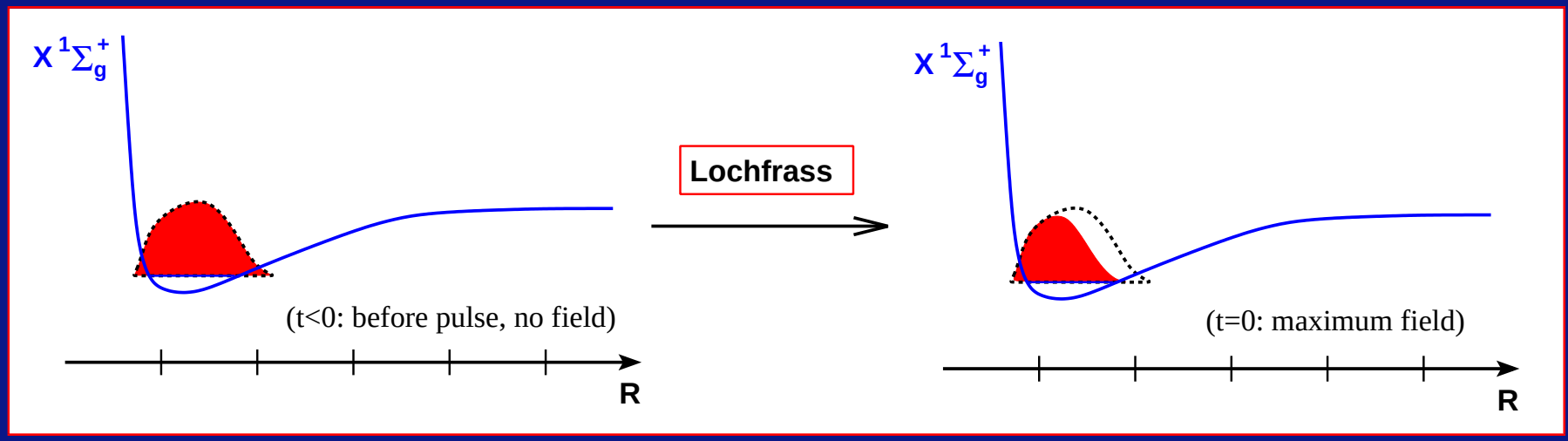

Strong-Field Control: "Lochfrass" (Proposal)

- **Pronounced R-dependent ionization yield**
  $\longrightarrow$ **fast** ionization process (pump) should **deplete** the large R component of the wavefunction.

- A coherent vibrational wavepacket in the **electronic ground state** of the **neutral(!)** molecule is created.

Strong-Field Control: "Lochfrass" (Proposal)

- **Pronounced R-dependent ionization yield**
  $\longrightarrow$ **fast** ionization process (pump) should **deplete** the large R component of the wavefunction.

- A coherent vibrational wavepacket in the **electronic ground state** of the **neutral(!)** molecule is created.

- **Purely quantum-mechanical effect:**
  A **Schrödinger cat** state of the **ionized** and the **neutral** molecule!

Strong-Field Control: "Lochfrass" (Proposal)

- **Pronounced R-dependent ionization yield**
  $\longrightarrow$ **fast** ionization process (pump) should **deplete** the large R component of the wavefunction.

- A coherent vibrational wavepacket in the **electronic ground state** of the **neutral(!)** molecule is created.

- **Purely quantum-mechanical effect:**
  A **Schrödinger cat** state of the **ionized** and the **neutral** molecule!

- **Absolutely non-resonant process:** very robust and quite independent on exact pulse shape, wavelength, phase . . .

Strong-Field Control: "Lochfrass" (Proposal)

- **Pronounced R-dependent ionization yield**
  $\longrightarrow$ **fast** ionization process (pump) should **deplete** the large R component of the wavefunction.

- A coherent vibrational wavepacket in the **electronic ground state** of the **neutral(!)** molecule is created.

- **Purely quantum-mechanical effect:**
  A **Schrödinger cat** state of the **ionized** and the **neutral** molecule!

- **Absolutely non-resonant process:** very robust and quite independent on exact pulse shape, wavelength, phase . . .

- **Highly non-linear process:**
  A second (probe) pulse should detect a time-dependent ionization signal.

Wave-packet study (results)

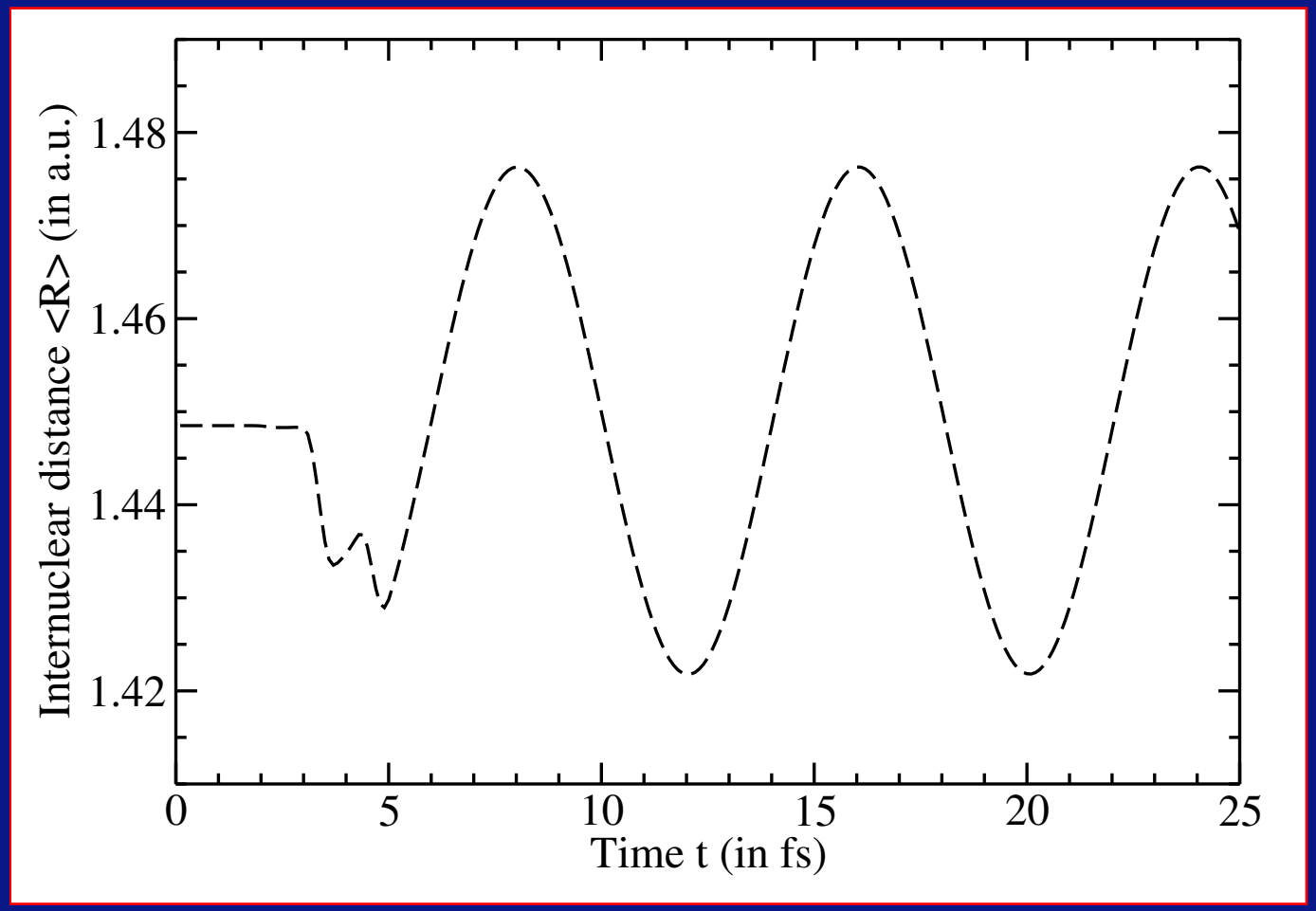

Peak intensity: $I = 6 \cdot 10^{14}\,\mathrm{W/cm^2}$, Wavelength: $\lambda = 800\,\mathrm{nm}$, Length: 8 fs.

Formation of a H_2 wavepacket by "Lochfrass" ("eating a hole").

Wave-packet detection: Pump-probe

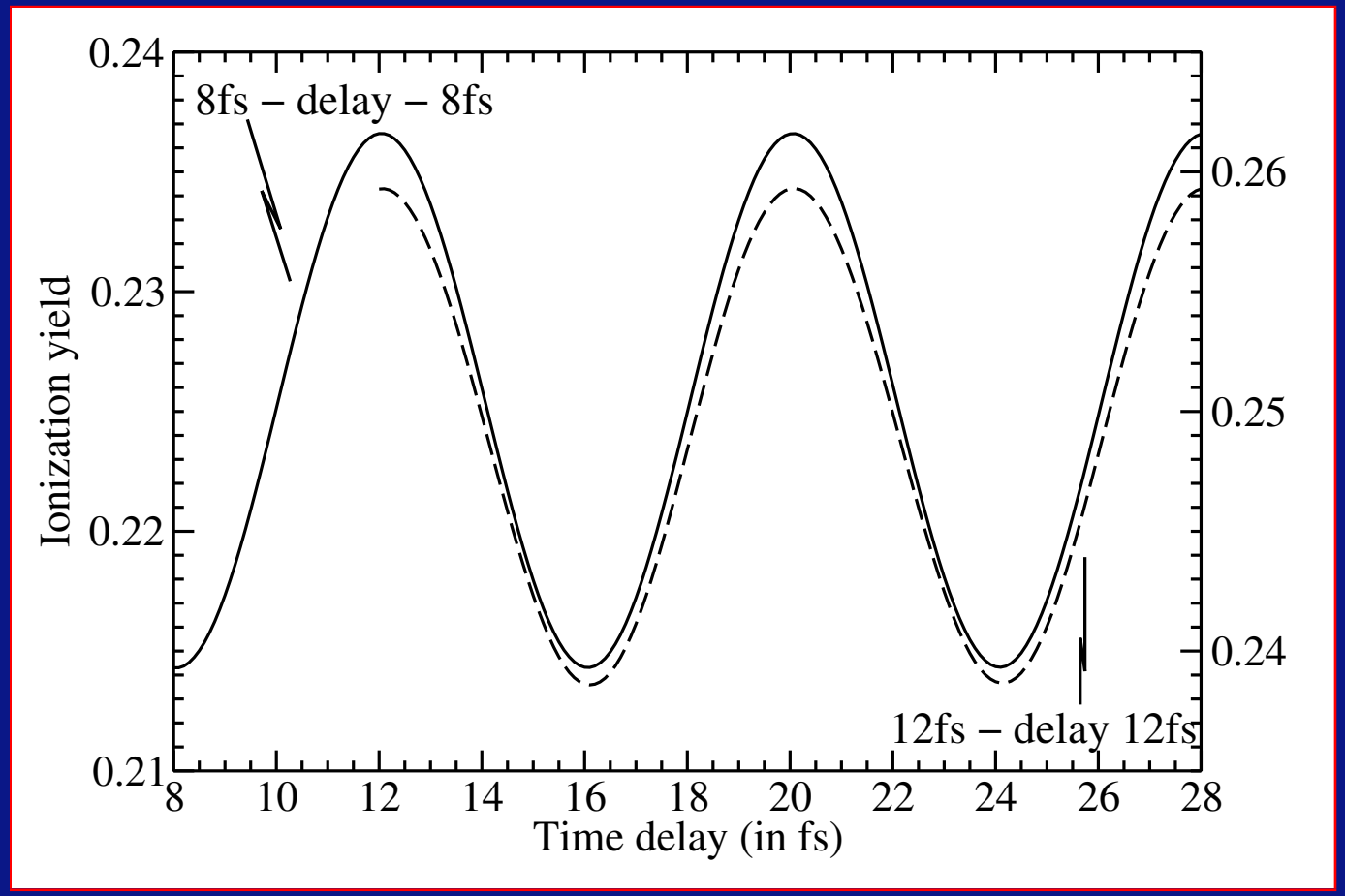

Identical pulses, Peak intensities: $I = 6 \cdot 10^{14}\,\mathrm{W/cm^2}$, Wavelength: $\lambda = 800\,\mathrm{nm}$.

[E. Goll, G. Wunner, and A. Saenz, *Phys. Rev. Lett.* **97**, 103003 (2006)]

Pump-probe experiment (MPI Heidelberg)

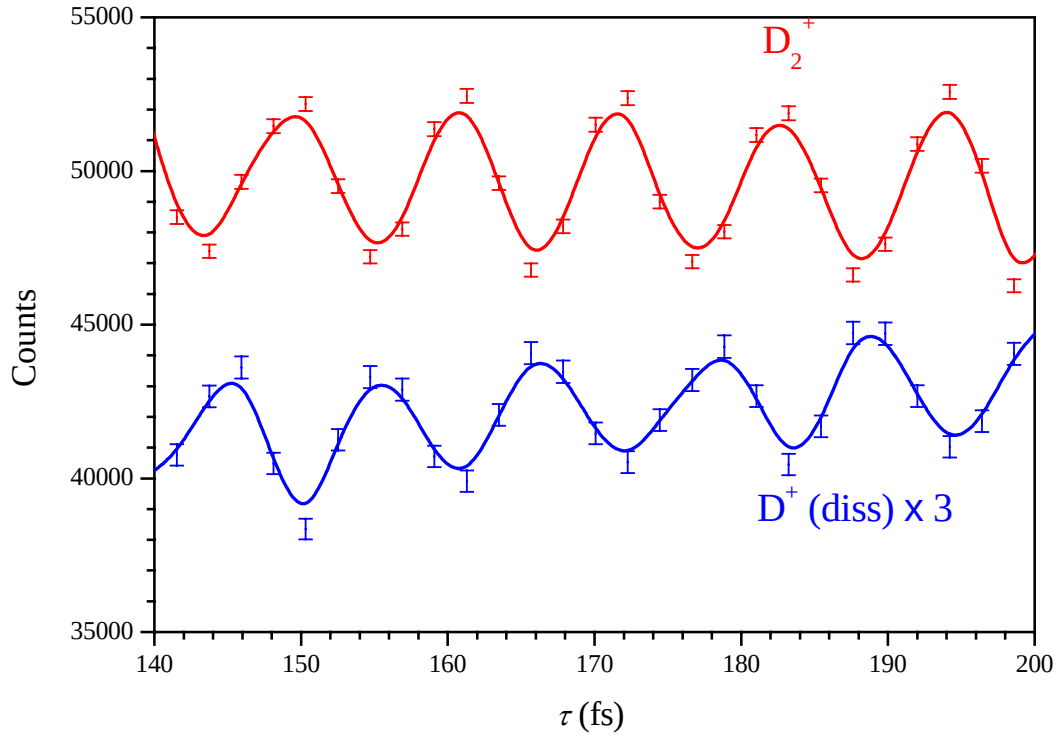

Figure 2

Parameters:

Two identical pulses,

$I = 4(1) \cdot 10^{14} \frac{\mathrm{W}}{\mathrm{cm}^2}$,

$\lambda = 795\,\mathrm{nm}$,

7 fs (FWHM).

[Fig. from Ergler et al. *Phys. Rev. Lett.* **97**, 103004 (2006)]

$\longrightarrow$ **Experiment observes the theoretically predicted oscillation!!!**

[**Note:** expected oscillation period for $\mathbf{D_2}$: 11 fs ($\mathbf{H_2}$: 8 fs).]

Strong-Field Control: "Lochfrass" (summary)

In the case of H_2 (D_2):

- Rather simple $v = 0$ and $v = 1$ vibrational wavepacket.

Strong-Field Control: "Lochfrass" (summary)

In the case of H_2 (D_2):

- Rather simple $v = 0$ and $v = 1$ vibrational wavepacket.
- Resulted in fastest vibrational motion observed so far (faster than the one in H_2^+).

Strong-Field Control: "Lochfrass" (summary)

In the case of H_2 (D_2):

- Rather simple $v = 0$ and $v = 1$ vibrational wavepacket.
- Resulted in fastest vibrational motion observed so far (faster than the one in H_2^+).
- Extremely long-lived wavepacket (vibrational deexcitation requires two-photon transition):

  $\longrightarrow$ **"molecular clock" or "pendulum".**

Strong-Field Control: "Lochfrass" (summary)

In the case of H_2 (D_2):

- Rather simple $v = 0$ and $v = 1$ vibrational wavepacket.
- Resulted in fastest vibrational motion observed so far (faster than the one in H_2^+).
- Extremely long-lived wavepacket (vibrational deexcitation requires two-photon transition):

  $\longrightarrow$ **"molecular clock" or "pendulum".**

For other molecular systems:

- Occurrence of "Lochfrass": whenever there is a (clear) nuclear-geometry dependence of the difference between the electronic ground state (hyper-)potential surfaces of the neutral and the ion.

Strong-Field Control: "Lochfrass" (summary)

In the case of H_2 (D_2):

- Rather simple $v = 0$ and $v = 1$ vibrational wavepacket.
- Resulted in fastest vibrational motion observed so far (faster than the one in H_2^+).
- Extremely long-lived wavepacket (vibrational deexcitation requires two-photon transition):

  $\longrightarrow$ **"molecular clock" or "pendulum".**

For other molecular systems:

- Occurrence of "Lochfrass": whenever there is a (clear) nuclear-geometry dependence of the difference between the electronic ground state (hyper-)potential surfaces of the neutral and the ion.
- For larger molecules "Lochfrass" may excite different **coupled** vibrational modes and allows their **real-time** observation.

[E. Goll, G. Wunner, and A. Saenz, *Phys. Rev. Lett.* **97**, 103003 (2006)]

Lochfraß in NH_3

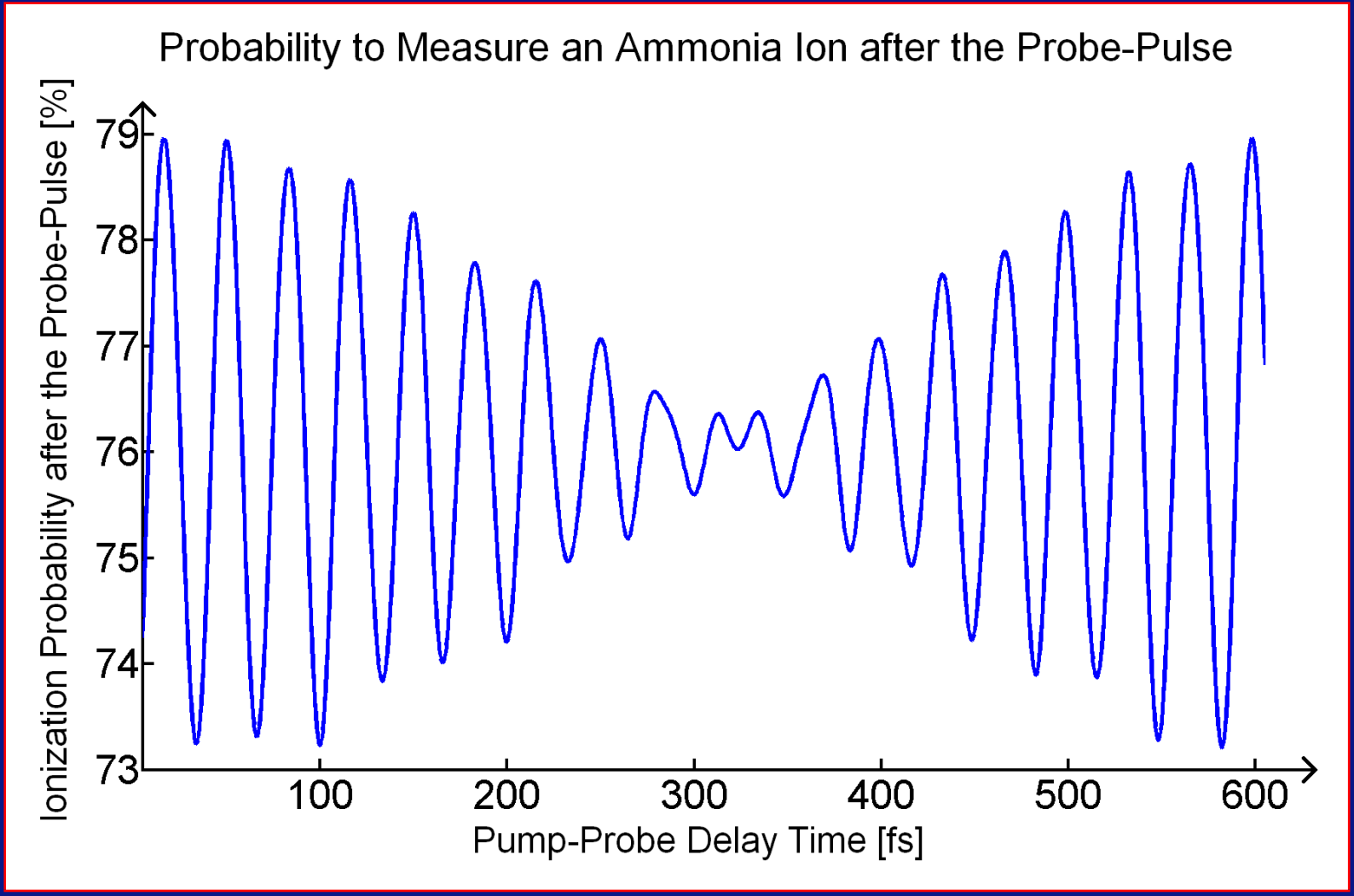

[J. Förster, A.S., *in preparation.*]

Alternative scheme based on high harmonics (PACER)

Real-time observation of nuclear motion using high harmonics.

Concept (M. Lein PRL 94, 053004 (2005)):

1. Unique mapping of high harmonic photon frequency ω on emission time t (within three-step model and for one cycle).

Alternative scheme based on high harmonics (PACER)

Real-time observation of nuclear motion using high harmonics.

Concept (M. Lein PRL 94, 053004 (2005)):

1. Unique mapping of high harmonic photon frequency ω on emission time t (within three-step model and for one cycle).

2. High-harmonic spectrum:

$$S_{\mathrm{mol}}(\omega) \;=\; \sum_{\alpha} \left|C_\alpha(\omega)\right|^2 s_\alpha(\omega)$$

   with orbital contribution $s_\alpha(\omega) = \int_{-\infty}^{\infty} \mathrm{d}t\, e^{i\omega t}\, \omega\, d_\alpha(t)$ with the dipole-expectation value $d_\alpha(t)$ for the time-dependent orbital α and

   the nuclear correlation function $C_\alpha(t) = \langle\, \chi(t=0) \,|\, \tilde{\chi}^{(+)}(t) \,\rangle$ between the nuclear wavefunctions of the neutral (χ) and the ion ($\tilde{\chi}_\alpha^{(+)}$).

Alternative scheme based on high harmonics (PACER)

Real-time observation of nuclear motion using high harmonics.

Concept (M. Lein PRL 94, 053004 (2005)):

1. Unique mapping of high harmonic photon frequency ω on emission time t (within three-step model and for one cycle).

2. High-harmonic spectrum:

$$S_{\mathrm{mol}}(\omega) \;=\; \sum_{\alpha} \left|C_\alpha(\omega)\right|^2 s_\alpha(\omega)$$

   with orbital contribution $s_\alpha(\omega) = \int_{-\infty}^{\infty} \mathrm{d}t\, e^{i\omega t}\, \omega\, d_\alpha(t)$ with the dipole-expectation value $d_\alpha(t)$ for the time-dependent orbital α and

   the nuclear correlation function $C_\alpha(t) = \langle\, \chi(t=0) \,|\, \tilde{\chi}^{(+)}(t) \,\rangle$ between the nuclear wavefunctions of the neutral (χ) and the ion ($\tilde{\chi}_\alpha^{(+)}$).

3. Taking the ratio for a molecule and its isotope-substituted counterpart, e. g. H_2O and D_2O, cancels electronic part $s_\alpha(\omega)$.

Nuclear Imaging with PACER

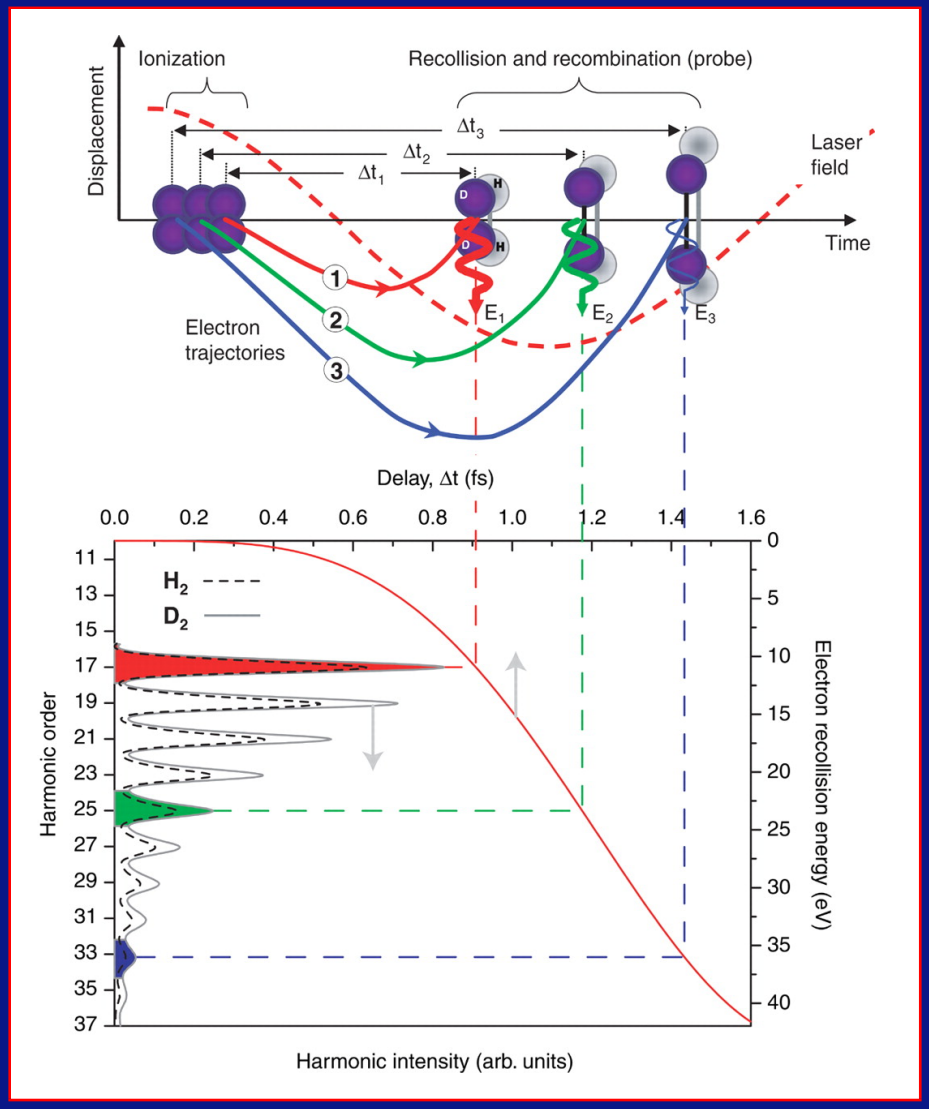

[S. Baker *et al.*, Science **312**, 424 (2006)]

PACER: Scheme and application example (H_2/D_2)

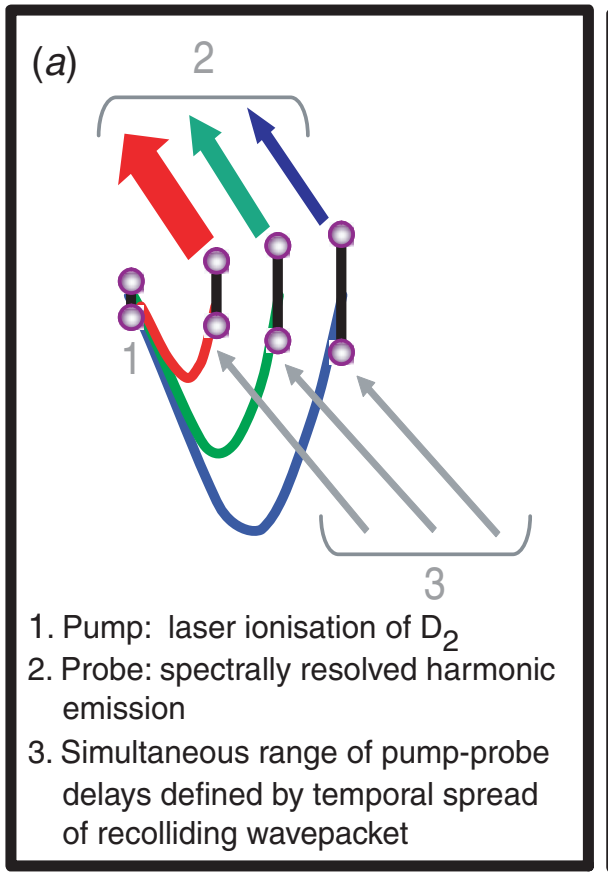

1. Pump: laser ionisation of D_2
2. Probe: spectrally resolved harmonic emission
3. Simultaneous range of pump-probe delays defined by temporal spread of recolliding wavepacket

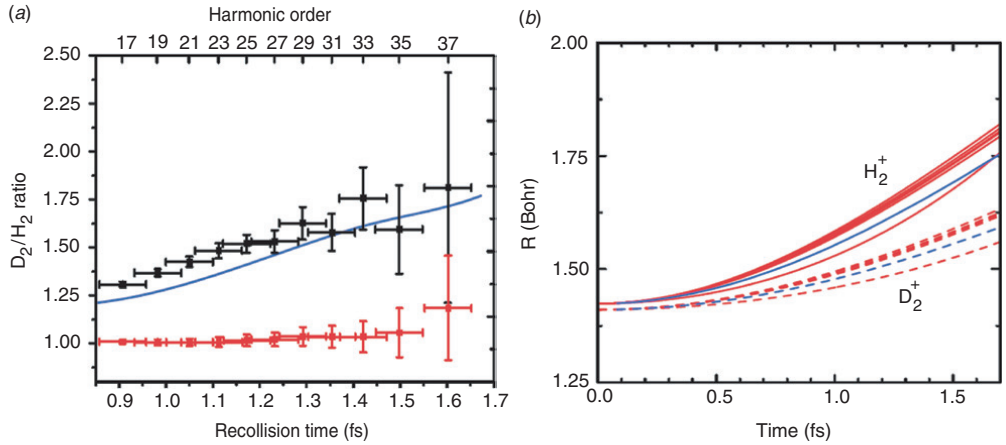

[Figures taken from S. Baker et al., *J. Mod. Optics* **54**, 1011 (2007).
(left original:) S. Baker et al., *Science* **312**, 424 (2005)]

Remarks on the PACER method:

- Observation of the (field-induced) motion in the formed ion,

  more accurately the autocorrelation function of the ionic wavepacket with the initial-state wavefunction.

Remarks on the PACER method:

- Observation of the (field-induced) motion in the formed ion,

  more accurately the autocorrelation function of the ionic wavepacket with the initial-state wavefunction.

- For such motion to occur, there must be a strongly nuclear-geometry dependent ionization probability as for "Lochfraß".

Remarks on the PACER method:

- Observation of the (field-induced) motion in the formed ion,

  more accurately the autocorrelation function of the ionic wavepacket with the initial-state wavefunction.

- For such motion to occur, there must be a strongly nuclear-geometry dependent ionization probability as for "Lochfraß".

- Requires isotope substitution (in the "relevant", i. e. the active vibration(s)).

Remarks on the PACER method:

- Observation of the (field-induced) motion in the formed ion,

  more accurately the autocorrelation function of the ionic wavepacket with the initial-state wavefunction.

- For such motion to occur, there must be a strongly nuclear-geometry dependent ionization probability as for "Lochfraß".

- Requires isotope substitution (in the "relevant", i. e. the active vibration(s)).

- Harmonic frequency to (emission) time mapping is only within a short time interval (half cycle of driving laser photons) possible: short time window for observation ($\approx 1.5\,$fs at 800 nm)

  $\longrightarrow$ longer wavelengths extend the time window.

PACER on NH_3 (I)

- **PACER experiment** on NH_3 and ND_3 with 1800 nm radiation [P. M. Kraus and H. J. Wörner, *ChemPhysChem* **14**, 1445 (2013)]: monotonically increasing ratio is found (as for H_2/D_2, CH_4/CD_4, H_2O/D_2O).

PACER on NH_3 (I)

- **PACER experiment** on NH_3 and ND_3 with 1800 nm radiation
  [P. M. Kraus and H. J. Wörner, *ChemPhysChem* **14**, 1445 (2013)]:
  monotonically increasing ratio is found (as for H_2/D_2, CH_4/CD_4, H_2O/D_2O).

- **Theoretical simulation** using a reduced-dimensionality model
  [J. Förster und A.S., *ChemPhysChem* **14**, 1438 (2013)]:
  good agreement with the experimental result is found,

PACER on NH_3 (I)

- **PACER experiment** on NH_3 and ND_3 with 1800 nm radiation
  [P. M. Kraus and H. J. Wörner, *ChemPhysChem* **14**, 1445 (2013)]:
  monotonically increasing ratio is found (as for H_2/D_2, CH_4/CD_4, H_2O/D_2O).

- **Theoretical simulation** using a reduced-dimensionality model
  [J. Förster und A.S., *ChemPhysChem* **14**, 1438 (2013)]:
  good agreement with the experimental result is found,
  but non-monotonically ratio predicted for later times.

PACER on NH_3 (I)

- **PACER experiment** on NH_3 and ND_3 with 1800 nm radiation
  [P. M. Kraus and H. J. Wörner, *ChemPhysChem* **14**, 1445 (2013)]:
  monotonically increasing ratio is found (as for H_2/D_2, CH_4/CD_4, H_2O/D_2O).

- **Theoretical simulation** using a reduced-dimensionality model
  [J. Förster und A.S., *ChemPhysChem* **14**, 1438 (2013)]:
  good agreement with the experimental result is found,
  but non-monotonically ratio predicted for later times.

- **Model:** Nuclear motion along the inversion coordinate x in the cation after the ionization step

$$\hat{\mathrm{H}}_{\mathrm{neutral}} = \frac{1}{2}\,\hat{\mathrm{p}}\frac{1}{\mu(x)}\hat{\mathrm{p}} + V_{\mathrm{neutral}}(x)$$

$$\hat{\mathrm{H}}_{\mathrm{ion}} = \frac{\hat{\mathrm{p}}^2}{2\mu} + V_{\mathrm{ion}}(x)$$

PACER on NH_3 (II)

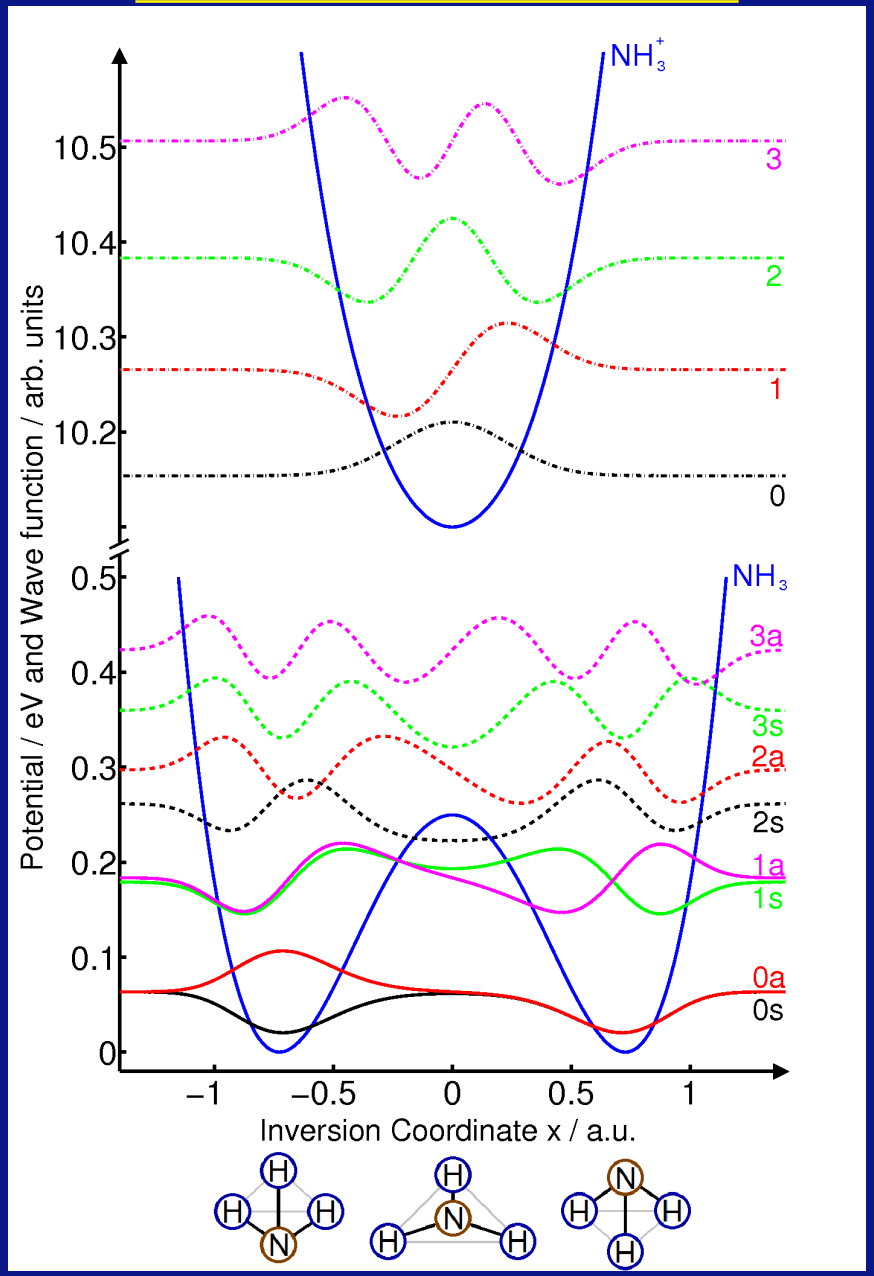

PACER on NH_3 (III)

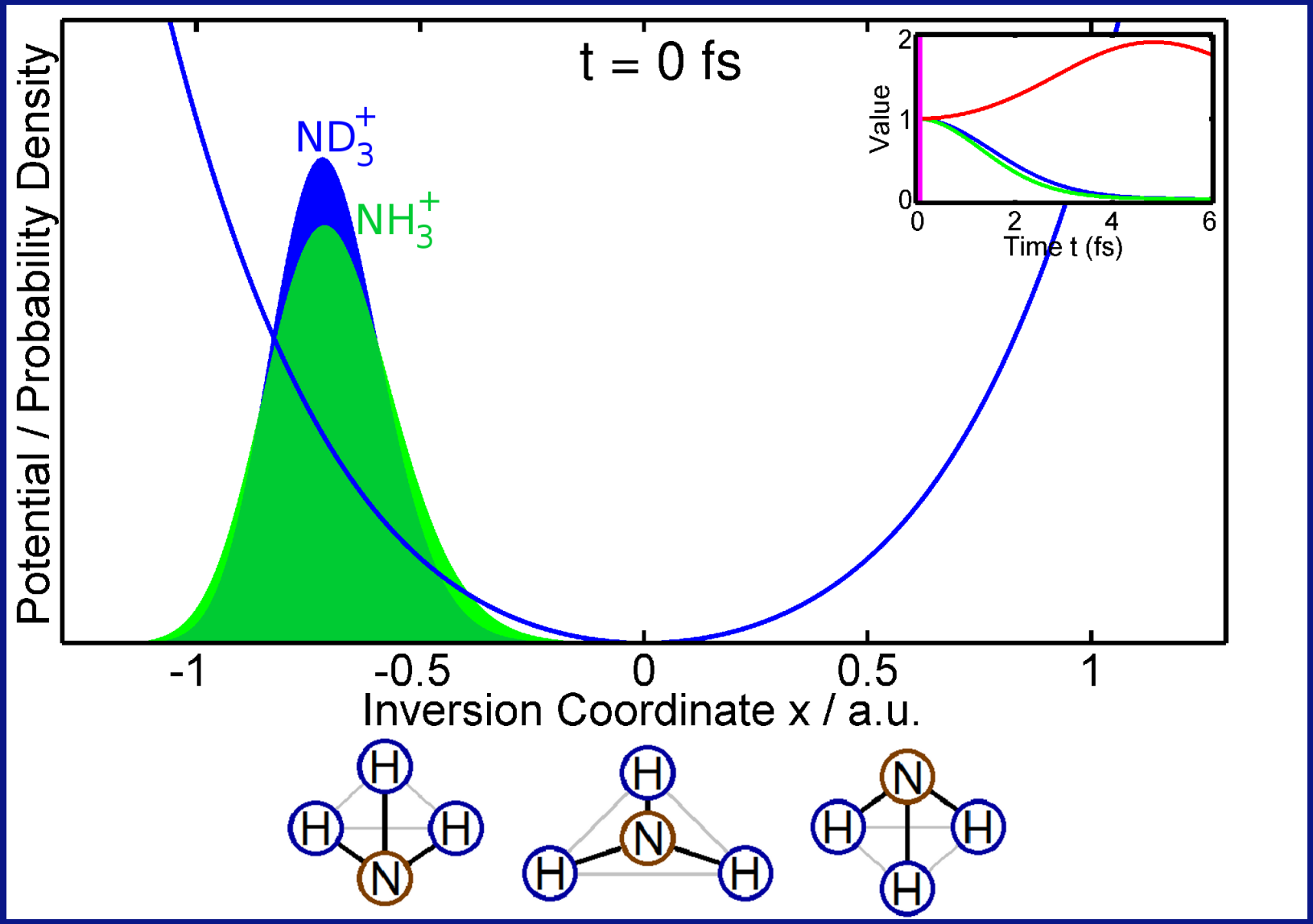

[J. Förster und A.S., *ChemPhysChem* **14**, 1438 (2013)]

PACER on NH_3 (III)

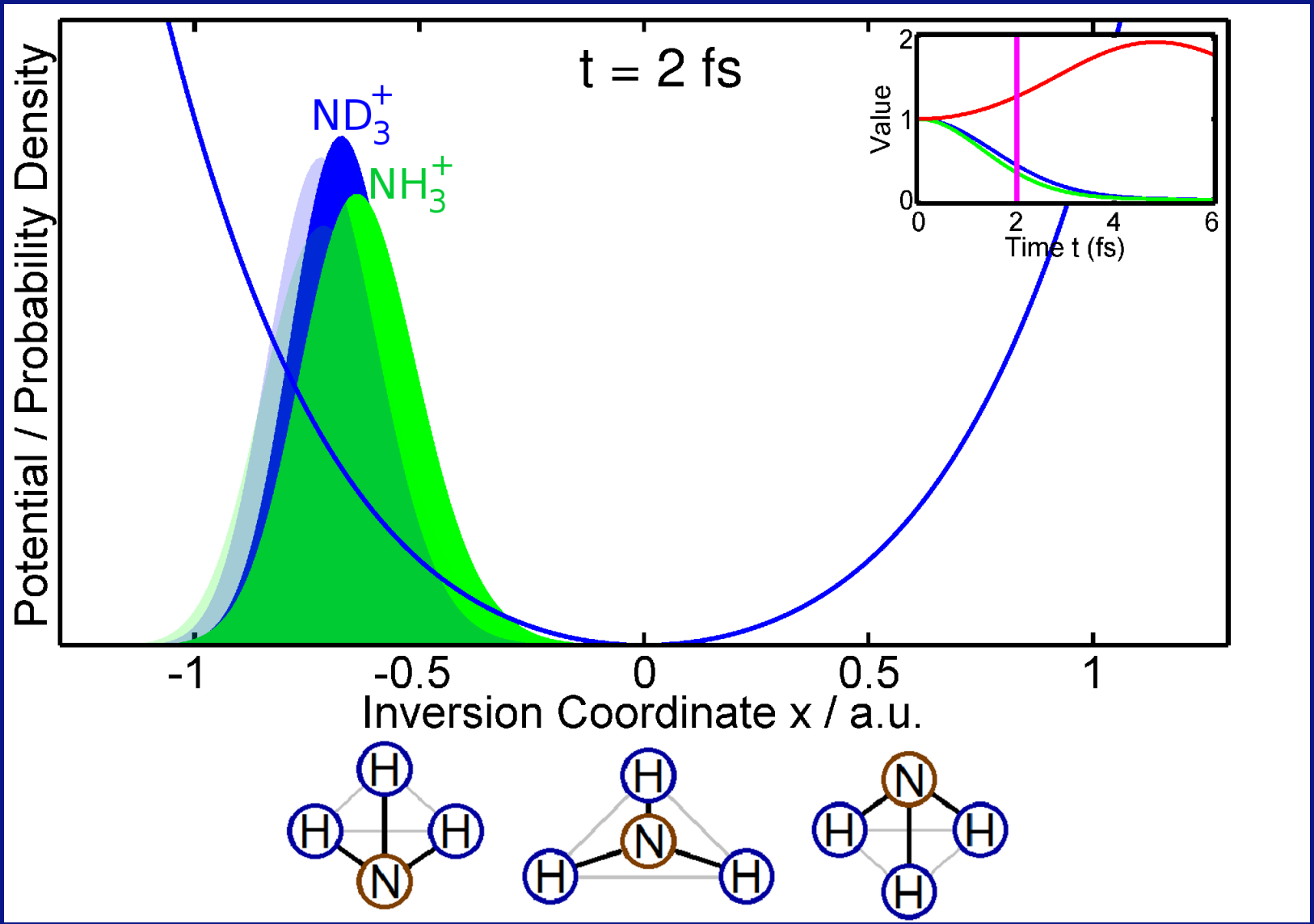

[J. Förster und A.S., *ChemPhysChem* **14**, 1438 (2013)]

PACER on NH_3 (III)

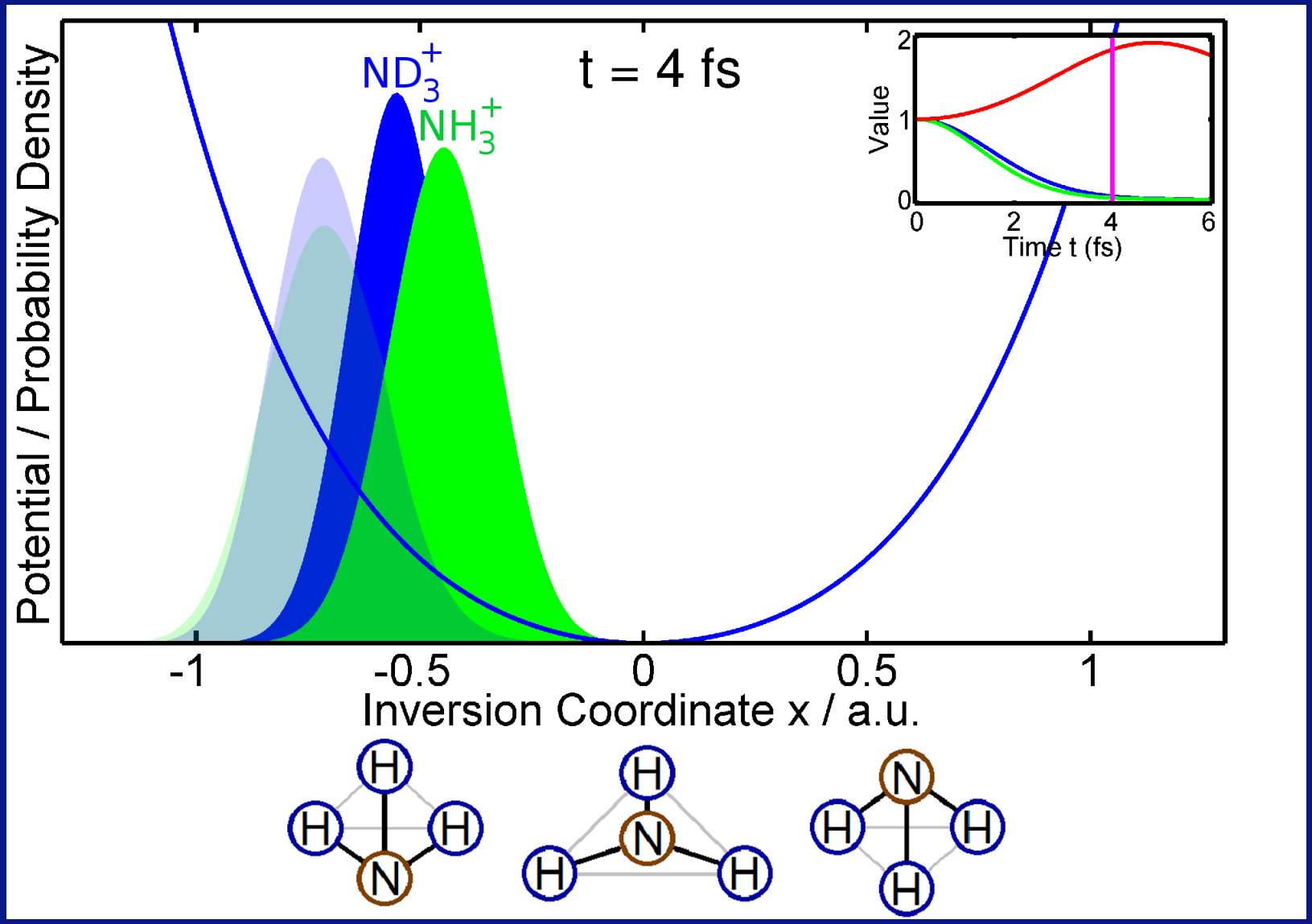

[J. Förster und A. Saenz, *ChemPhysChem* **14**, 1438 (2013)]

PACER on NH_3 (III)

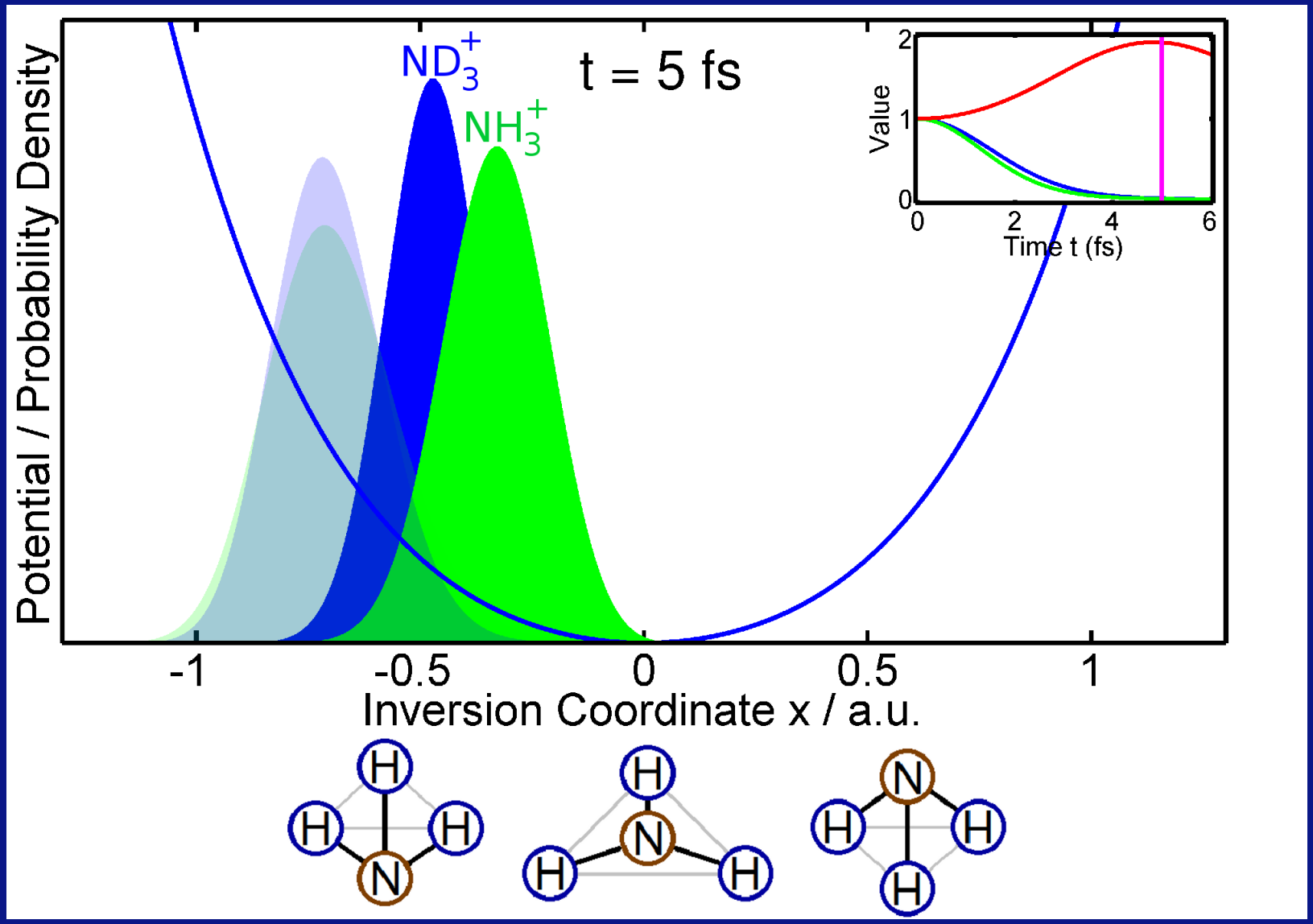

[J. Förster und A.S., *ChemPhysChem* **14**, 1438 (2013)]

PACER on NH_3 (III)

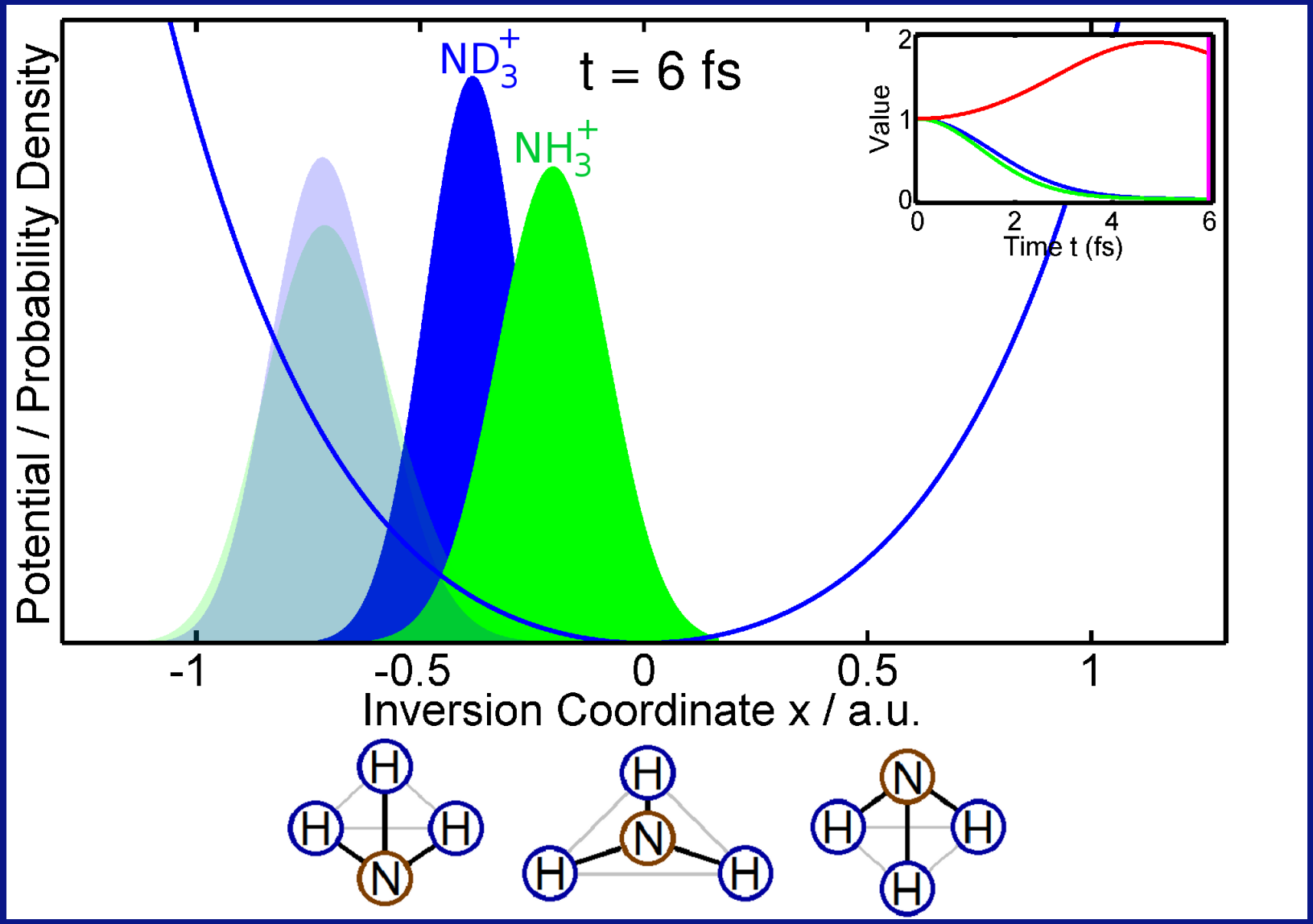

[J. Förster und A.S., *ChemPhysChem* **14**, 1438 (2013)]

PACER on NH_3 (IV): long-time behavior

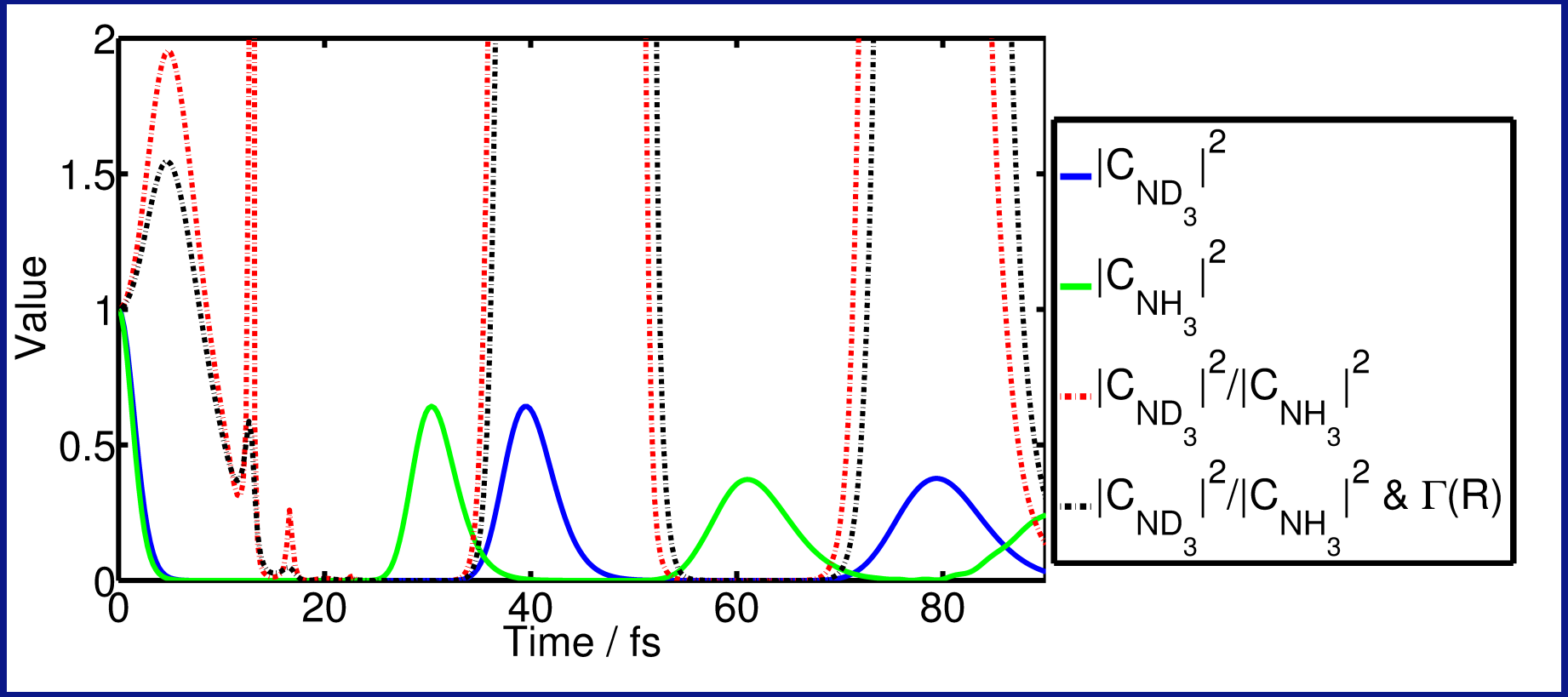

[J. Förster und A.S., *ChemPhysChem* **14**, 1438 (2013)]

A closer look at the autocorrelation function (I)

- Needed: nuclear autocorrelation function

$$C(t) \;=\; \langle \Psi_{\mathrm{neutral}}(t=0) | \Phi_{\mathrm{ion}}(t) \rangle$$

A closer look at the autocorrelation function (I)

- Needed: nuclear autocorrelation function

$$C(t) \;=\; \langle \Psi_{\mathrm{neutral}}(t=0) | \Phi_{\mathrm{ion}}(t) \rangle$$

- Ionic wave packet expressed in the stationary ionic eigenstates $\left| \tilde{\Phi}_{n,\mathrm{ion}} \right\rangle$:

$$|\Phi_{\mathrm{ion}}(t)\rangle = \sum_n c_n \left| \tilde{\Phi}_{n,\mathrm{ion}} \right\rangle \exp\left(-i \frac{\mathrm{E}_n}{\hbar} t \right)$$

A closer look at the autocorrelation function (I)

- Needed: nuclear autocorrelation function

$$C(t) \;=\; \langle \Psi_{\mathrm{neutral}}(t=0) | \Phi_{\mathrm{ion}}(t) \rangle$$

- Ionic wave packet expressed in the stationary ionic eigenstates $\left| \tilde{\Phi}_{n,\mathrm{ion}} \right\rangle$:

$$|\Phi_{\mathrm{ion}}(t)\rangle = \sum_n c_n \left| \tilde{\Phi}_{n,\mathrm{ion}} \right\rangle \exp\left(-i \frac{\mathrm{E}_n}{\hbar} t \right)$$

- This leads to the autocorrelation function

$$\begin{aligned} C(t) \;&=\; \langle \Psi_{\mathrm{neutral}}(t=0) | \Phi_{\mathrm{ion}}(t) \rangle \\ &= \sum_n c_n \left\langle \Psi_{\mathrm{neutral}}(t=0) \right| \left. \tilde{\Phi}_{n,\mathrm{ion}} \right\rangle \exp\left(-i \frac{\mathrm{E}_n}{\hbar} t \right) \end{aligned}$$

A closer look on the autocorrelation function (II)

$$C(t) \; = \sum_n c_n \left\langle \Psi_{\mathrm{neutral}}(t=0) \middle| \tilde{\Phi}_{n,\mathrm{ion}} \right\rangle \exp\left(-i\frac{\mathrm{E}_n}{\hbar}t\right)$$

- The coefficients c_n of the ionic wave packet come from the ionization step!

A closer look on the autocorrelation function (II)

$$C(t) = \sum_n c_n \left\langle \Psi_{\mathrm{neutral}}(t=0) \middle| \tilde{\Phi}_{n,\mathrm{ion}} \right\rangle \exp\left(-i\frac{\mathrm{E}_n}{\hbar}t\right)$$

- The coefficients c_n of the ionic wave packet come from the ionization step!
- Franck-Condon: $c_n^{\mathrm{FC}} = \left\langle \tilde{\Phi}_{n,\mathrm{ion}} \middle| \Psi_{\mathrm{neutral}}(t=0) \right\rangle$

A closer look on the autocorrelation function (II)

$$C(t) = \sum_n c_n \left\langle \Psi_{\mathrm{neutral}}(t=0) \middle| \tilde{\Phi}_{n,\mathrm{ion}} \right\rangle \exp\left(-i\frac{\mathrm{E}_n}{\hbar}t\right)$$

- The coefficients c_n of the ionic wave packet come from the ionization step!
- Franck-Condon: $c_n^{\mathrm{FC}} = \left\langle \tilde{\Phi}_{n,\mathrm{ion}} \middle| \Psi_{\mathrm{neutral}}(t=0) \right\rangle$
- **Note:** in Franck-Condon approximation one finds:

$$C(t) = \sum_n c_n^{\mathrm{FC}} \left\langle \Psi_{\mathrm{neutral}}(t=0) \middle| \tilde{\Phi}_{n,\mathrm{ion}} \right\rangle \exp\left(-i\frac{\mathrm{E}_n}{\hbar}t\right) = \sum_n |c_n^{\mathrm{FC}}|^2 \exp\left(-i\frac{\mathrm{E}_n}{\hbar}t\right)$$

A closer look on the autocorrelation function (II)

$$C(t) = \sum_n c_n \left\langle \Psi_{\mathrm{neutral}}(t=0) \middle| \tilde{\Phi}_{n,\mathrm{ion}} \right\rangle \exp\left(-i\frac{\mathrm{E}_n}{\hbar}t\right)$$

- The coefficients c_n of the ionic wave packet come from the ionization step!
- Franck-Condon: $c_n^{\mathrm{FC}} = \left\langle \tilde{\Phi}_{n,\mathrm{ion}} \middle| \Psi_{\mathrm{neutral}}(t=0) \right\rangle$
- **Note:** in Franck-Condon approximation one finds:

$$C(t) = \sum_n c_n^{\mathrm{FC}} \left\langle \Psi_{\mathrm{neutral}}(t=0) \middle| \tilde{\Phi}_{n,\mathrm{ion}} \right\rangle \exp\left(-i\frac{\mathrm{E}_n}{\hbar}t\right) = \sum_n |c_n^{\mathrm{FC}}|^2 \exp\left(-i\frac{\mathrm{E}_n}{\hbar}t\right)$$

- In Franck-Condon approximation, all necessary data are available from standard photoelectron spectroscopy!

A closer look on the autocorrelation function (III)

- **Strong-field ionization:** strong dependence of the ionization rate, e.g. $\Gamma(R) \propto \exp\left(-\frac{2}{3}\frac{(2I_p(R))^{3/2}}{F}\right)$, on nuclear geometry via $I_p(R)$

$$c_n^{\mathrm{SF}} \propto \left\langle \tilde{\Phi}_{n,\mathrm{ion}}(R) \middle| \Gamma^{\frac{1}{2}}(R) \middle| \Psi_{\mathrm{neutral}}(R, t=0) \right\rangle$$

A closer look on the autocorrelation function (III)

- **Strong-field ionization:** strong dependence of the ionization rate, e.g. $\Gamma(R) \propto \exp\left(-\frac{2}{3}\frac{(2I_p(R))^{3/2}}{F}\right)$, on nuclear geometry via $I_p(R)$

$$c_n^{\mathrm{SF}} \propto \left\langle \tilde{\Phi}_{n,\mathrm{ion}}(R) \middle| \Gamma^{\frac{1}{2}}(R) \middle| \Psi_{\mathrm{neutral}}(R, t=0) \right\rangle$$

- Further approximation (if wavefunction not available):

$$c_n^{\mathrm{SF,appr}} \propto \left\langle \tilde{\Phi}_{n,\mathrm{ion}} \middle| \Psi_{\mathrm{neutral}}(t=0) \right\rangle \Gamma^{\frac{1}{2}}(I_p(n)) = c_n^{\mathrm{FC}}\, \Gamma^{\frac{1}{2}}(I_p(n))$$

where $I_p(n) = I_p(0) + (E_n - E_0)$.

A closer look on the autocorrelation function (III)

- **Strong-field ionization:** strong dependence of the ionization rate, e.g. $\Gamma(R) \propto \exp\left(-\frac{2}{3}\frac{(2I_p(R))^{3/2}}{F}\right)$, on nuclear geometry via $I_p(R)$

$$c_n^{\mathrm{SF}} \propto \left\langle \tilde{\Phi}_{n,\mathrm{ion}}(R) \middle| \Gamma^{\frac{1}{2}}(R) \middle| \Psi_{\mathrm{neutral}}(R, t=0) \right\rangle$$

- Further approximation (if wavefunction not available):

$$c_n^{\mathrm{SF,appr}} \propto \left\langle \tilde{\Phi}_{n,\mathrm{ion}} \middle| \Psi_{\mathrm{neutral}}(t=0) \right\rangle \Gamma^{\frac{1}{2}}(I_p(n)) = c_n^{\mathrm{FC}} \, \Gamma^{\frac{1}{2}}(I_p(n))$$

  where $I_p(n) = I_p(0) + (E_n - E_0)$.

- Does this approximation work?

A closer look on the autocorrelation function (IV)

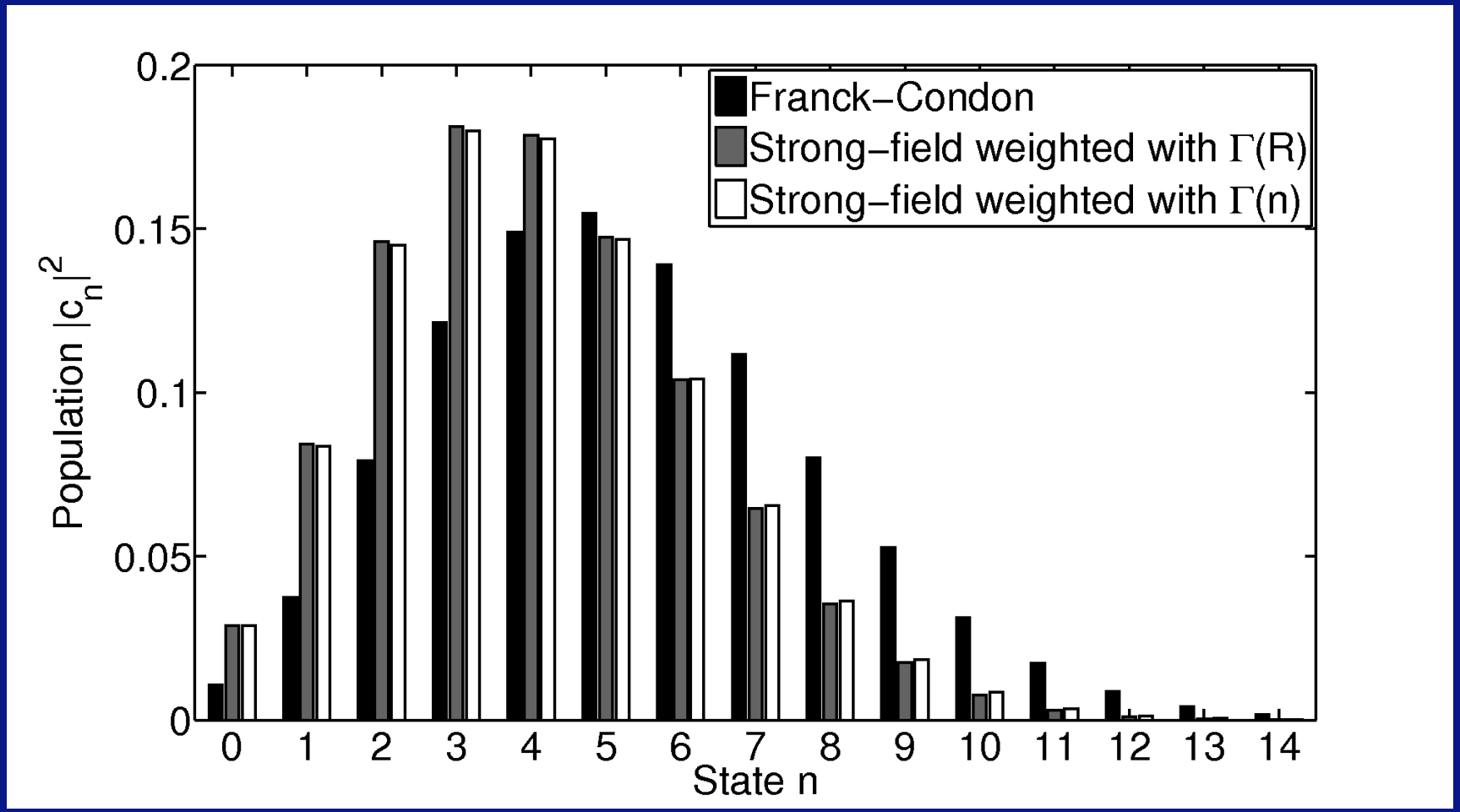

- practically no difference between the weighting with $\Gamma(R)$ and $\Gamma(n)$ (same for H_2), but $\Gamma(n)$ may be extracted from photoelectron spectra

A closer look on the autocorrelation function (V)

In conclusion, one may use

$$C(t) \;=\; \sum_{n} \; |c_n^{\mathrm{FC}}|^2 \; \Gamma^{\frac{1}{2}}(I_p(n)) \; \exp\left(-i\frac{\mathrm{E}_n}{\hbar}t\right)$$

where all data can be obtained from photoelectron spectra!

A closer look on the autocorrelation function (V)

In conclusion, one may use

$$C(t) \;=\; \sum_{n} \; |c_n^{\mathrm{FC}}|^2 \; \Gamma^{\frac{1}{2}}(I_p(n)) \; \exp\left(-i\frac{\mathrm{E}_n}{\hbar}t\right)$$

where all data can be obtained from photoelectron spectra!

That is great!

A closer look on the autocorrelation function (V)

In conclusion, one may use

$$C(t) \;=\; \sum_n \; |c_n^{\mathrm{FC}}|^2 \; \Gamma^{\frac{1}{2}}(I_p(n)) \; \exp\left(-i\frac{\mathrm{E}_n}{\hbar}t\right)$$

where all data can be obtained from photoelectron spectra!

That is great!

However, why does one need PACER, if all information is contained (for arbitrary time t!!!) in standard photoelectron spectra?

A closer look on the autocorrelation function (V)

In conclusion, one may use

$$C(t) \;=\; \sum_n \; |c_n^{\mathrm{FC}}|^2 \; \Gamma^{\frac{1}{2}}(I_p(n)) \; \exp\left(-i\frac{\mathrm{E}_n}{\hbar}t\right)$$

where all data can be obtained from photoelectron spectra!

That is great!

However, why does one need PACER, if all information is contained (for arbitrary time t!!!) in standard photoelectron spectra?

Only an additional time component like a chemical reaction makes it interesting!

Requires pump-probe schemes to initiate an (e.g. photochemical) time-dependent process.

H_2: low-intensity, high frequency regime

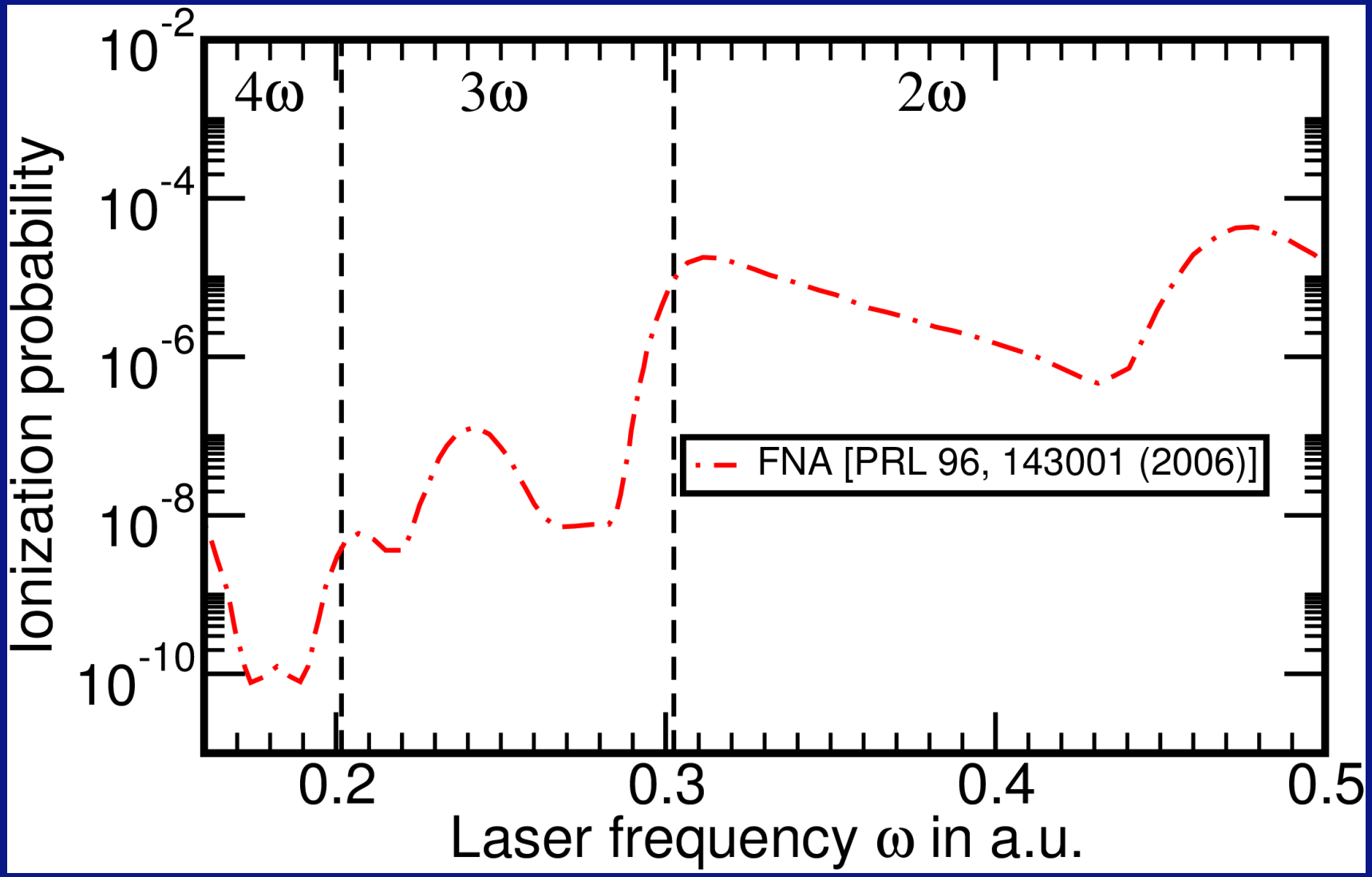

Ionization probability (frequency scan). Pulse parameters: duration $T = 10$ fs ($\cos^2$-envelope), peak intensity $I = 10^{12}$ W cm^{-2}, alignment: $\|$.

H_2: low-intensity, high frequency regime

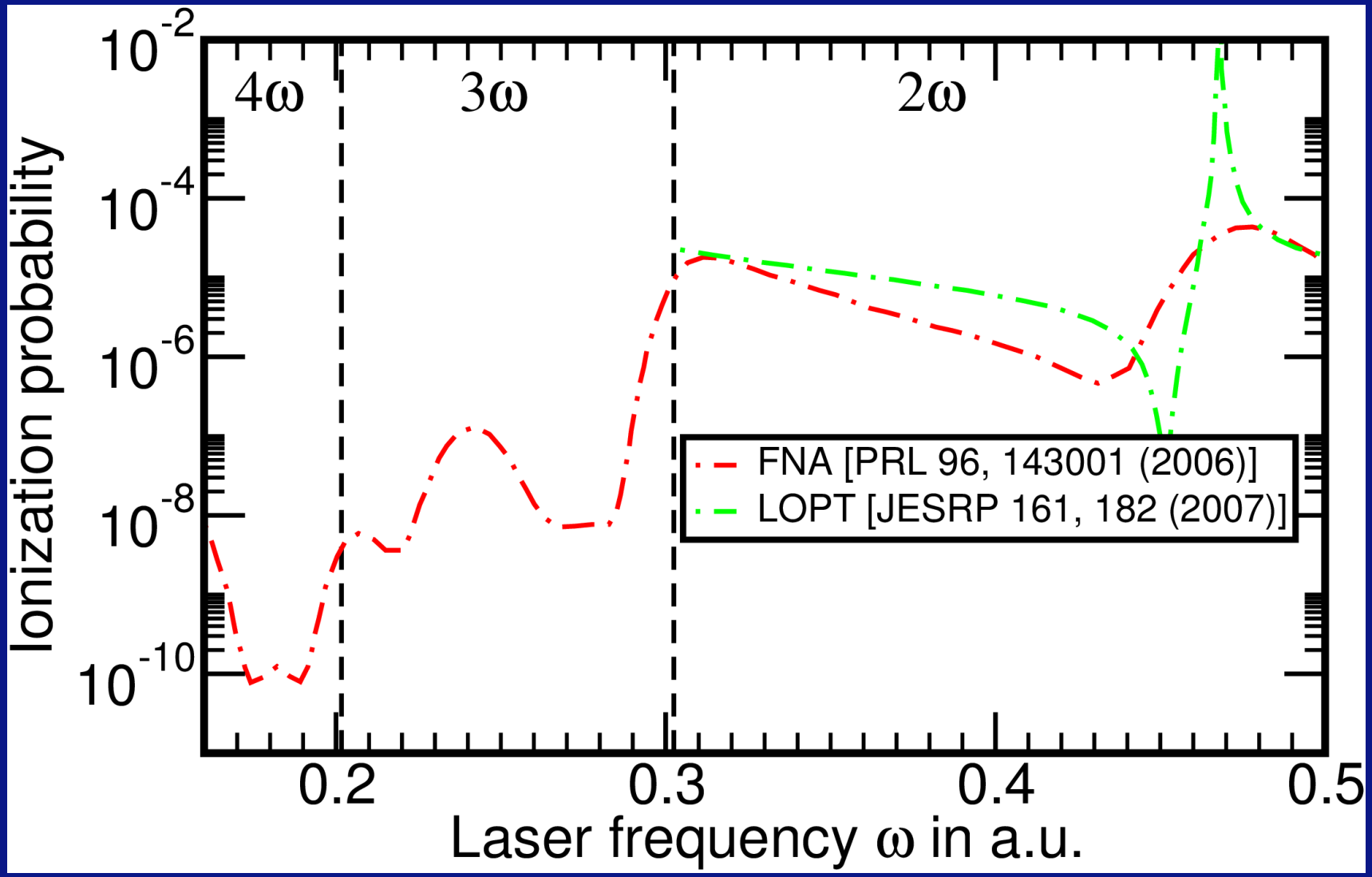

Ionization probability (frequency scan). Pulse parameters: duration $T = 10$ fs ($\cos^2$-envelope), peak intensity $I = 10^{12}$ W cm^{-2}, alignment: $\|$.

H_2: low-intensity, high frequency regime

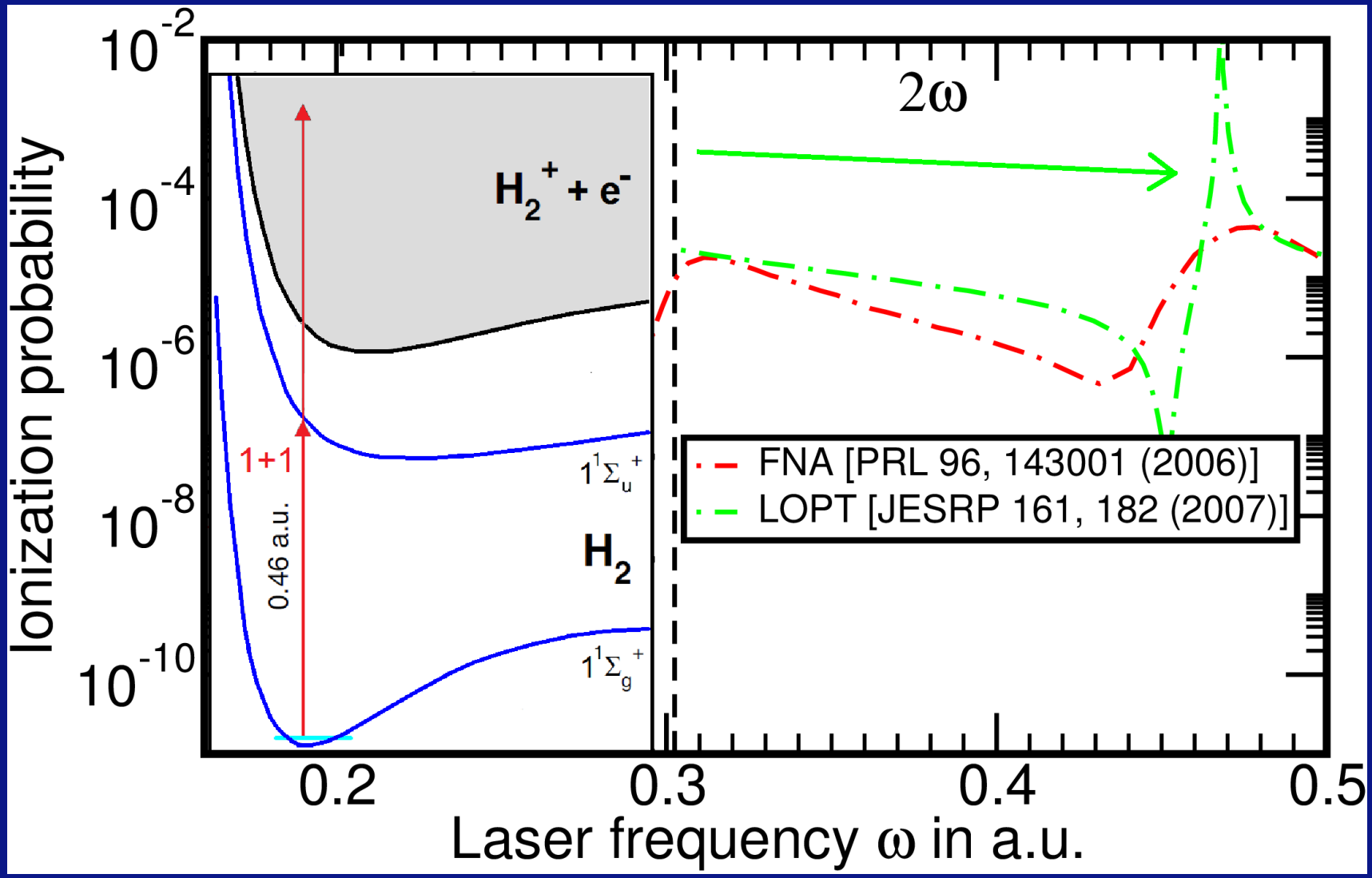

Ionization probability (frequency scan). Pulse parameters: duration $T = 10$ fs ($\cos^2$-envelope), peak intensity $I = 10^{12}$ W cm^{-2}, alignment: $\|$.

H_2: low-intensity, high frequency regime

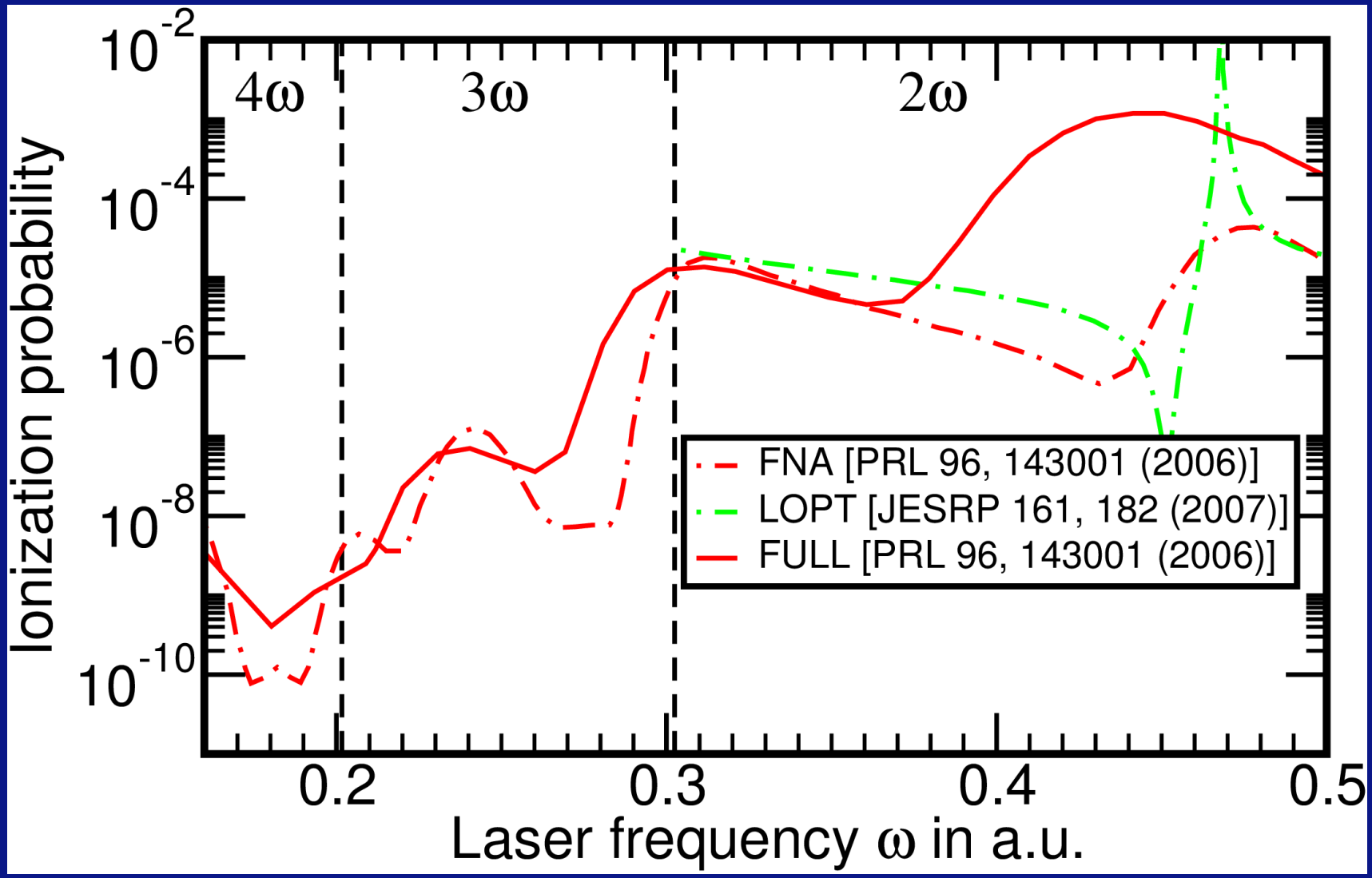

Ionization probability (frequency scan). Pulse parameters: duration $T = 10$ fs ($\cos^2$-envelope), peak intensity $I = 10^{12}$ W cm^{-2}, alignment: $\|$.

H_2: low-intensity, high frequency regime

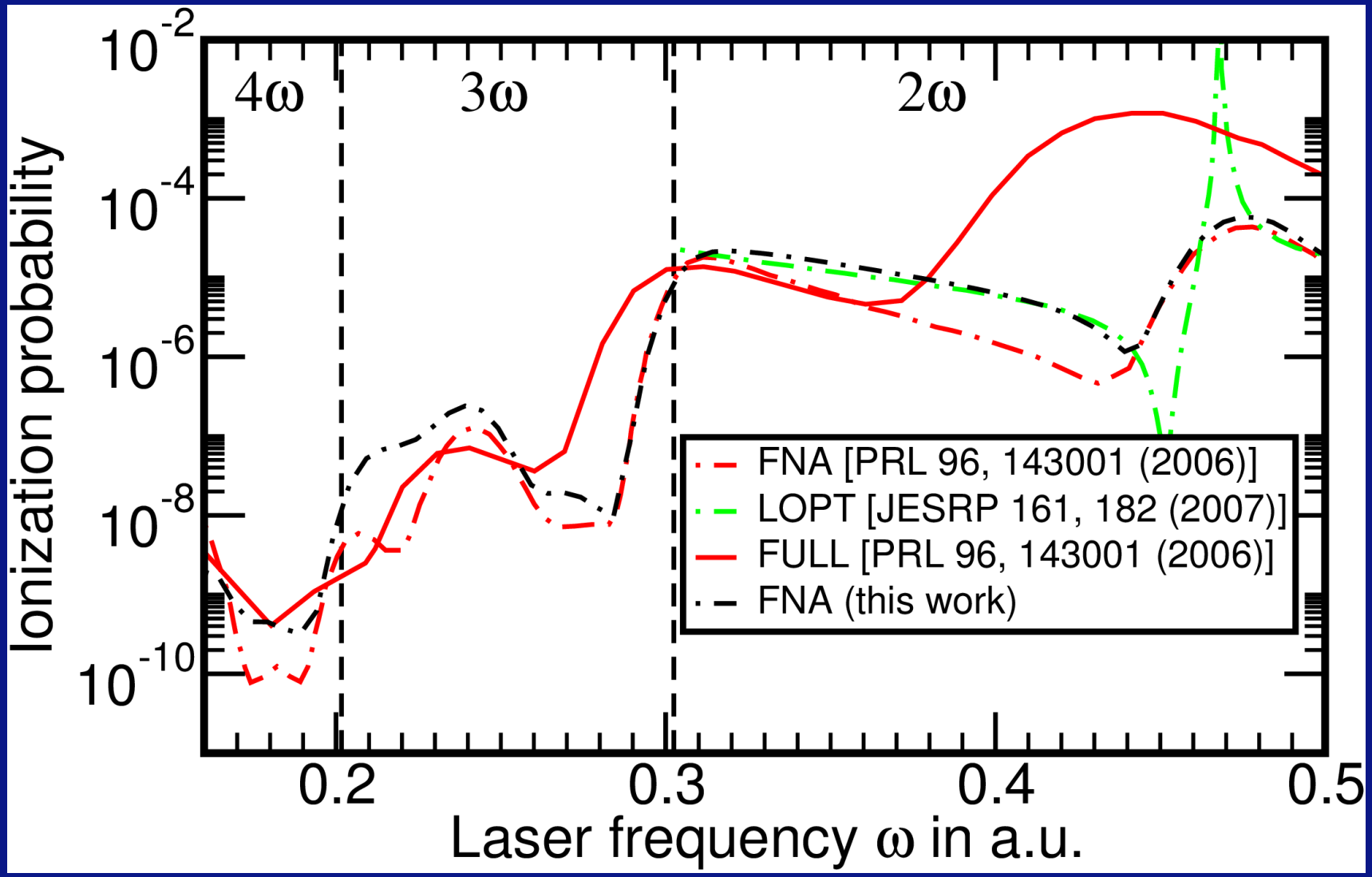

Ionization probability (frequency scan). Pulse parameters: duration $T = 10$ fs ($\cos^2$-envelope), peak intensity $I = 10^{12}$ W cm^{-2}, alignment: $\|$.

H_2: low-intensity, high frequency regime

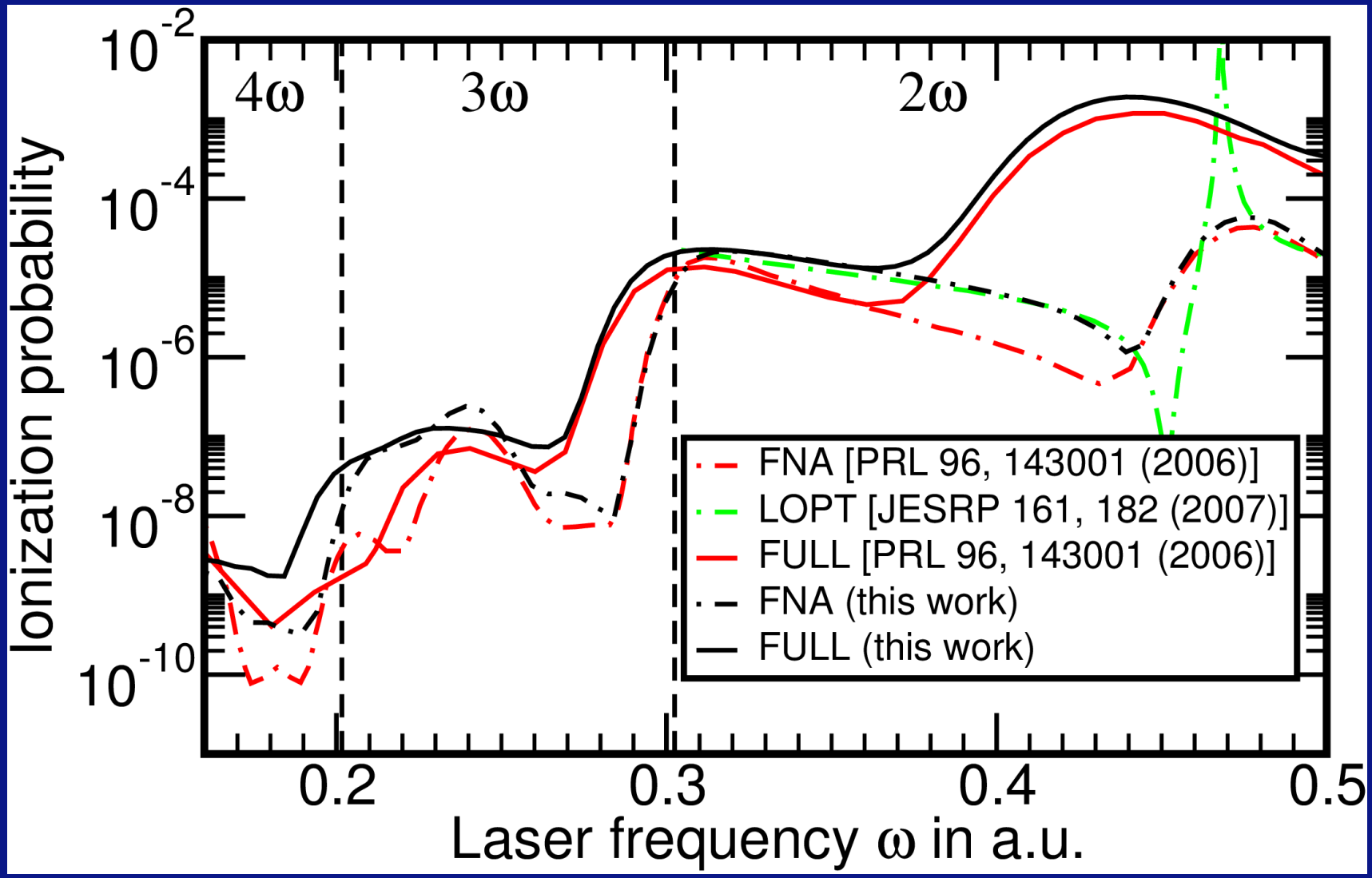

Ionization probability (frequency scan). Pulse parameters: duration $T = 10$ fs ($\cos^2$-envelope), peak intensity $I = 10^{12}$ W cm^{-2}, alignment: $\|$.

H_2: low-intensity, high frequency regime

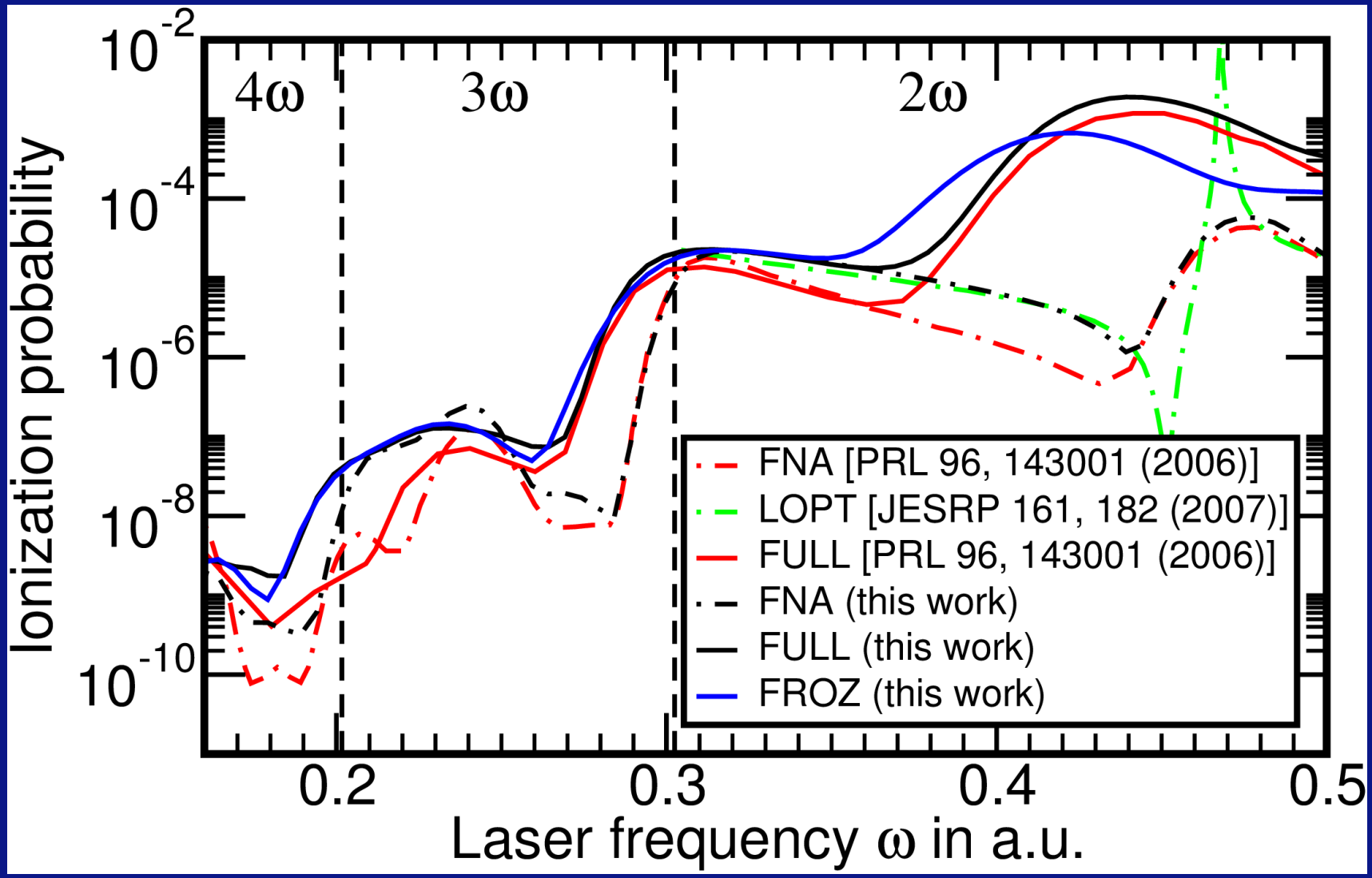

Ionization probability (frequency scan). Pulse parameters: duration $T = 10$ fs ($\cos^2$-envelope), peak intensity $I = 10^{12}$ W cm^{-2}, alignment: $\|$.

H_2: low-intensity, high frequency regime

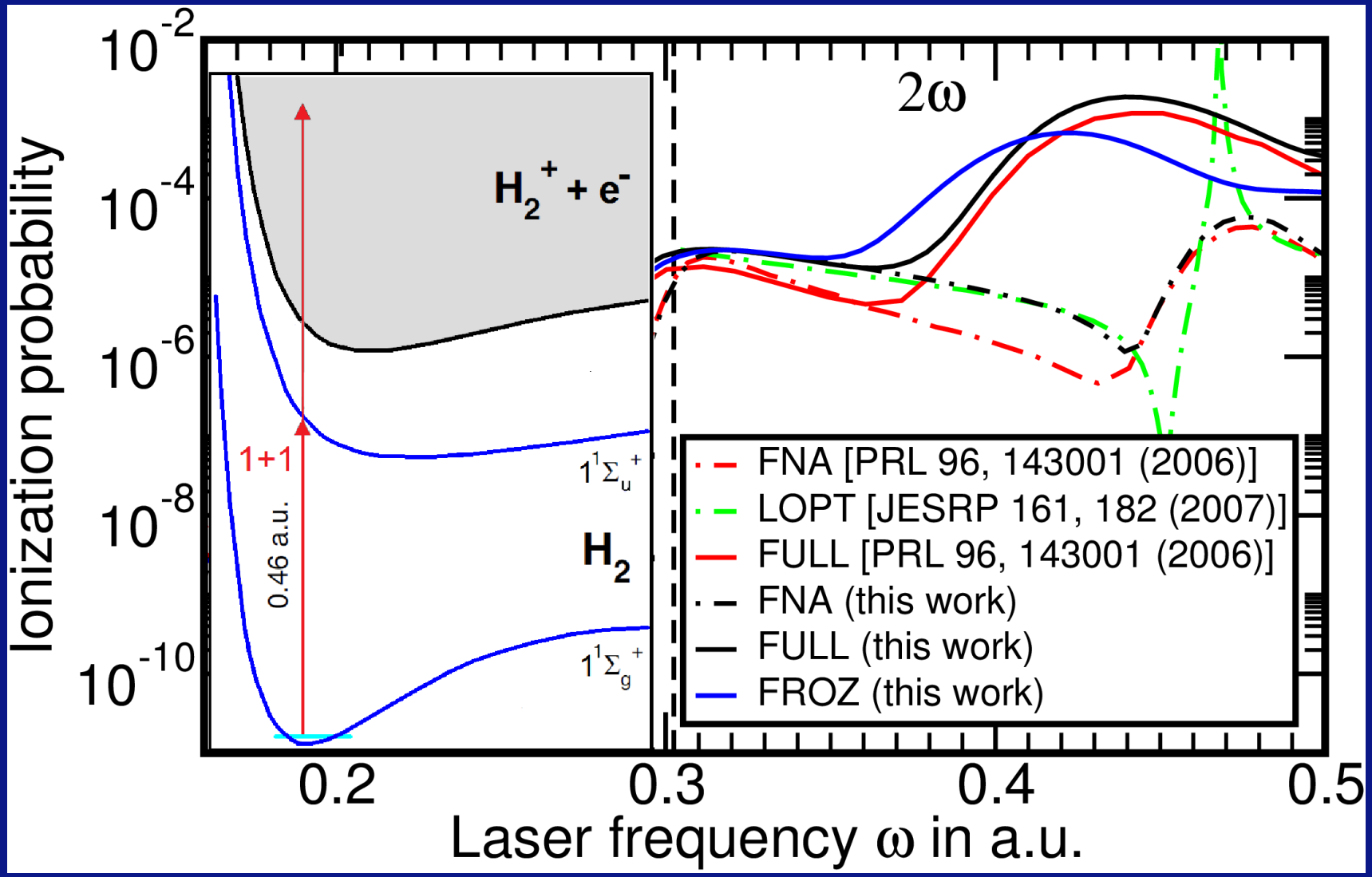

Ionization probability (frequency scan). Pulse parameters: duration $T = 10$ fs ($\cos^2$-envelope), peak intensity $I = 10^{12}$ W cm^{-2}, alignment: $\|$.

H_2: low-intensity, high frequency regime

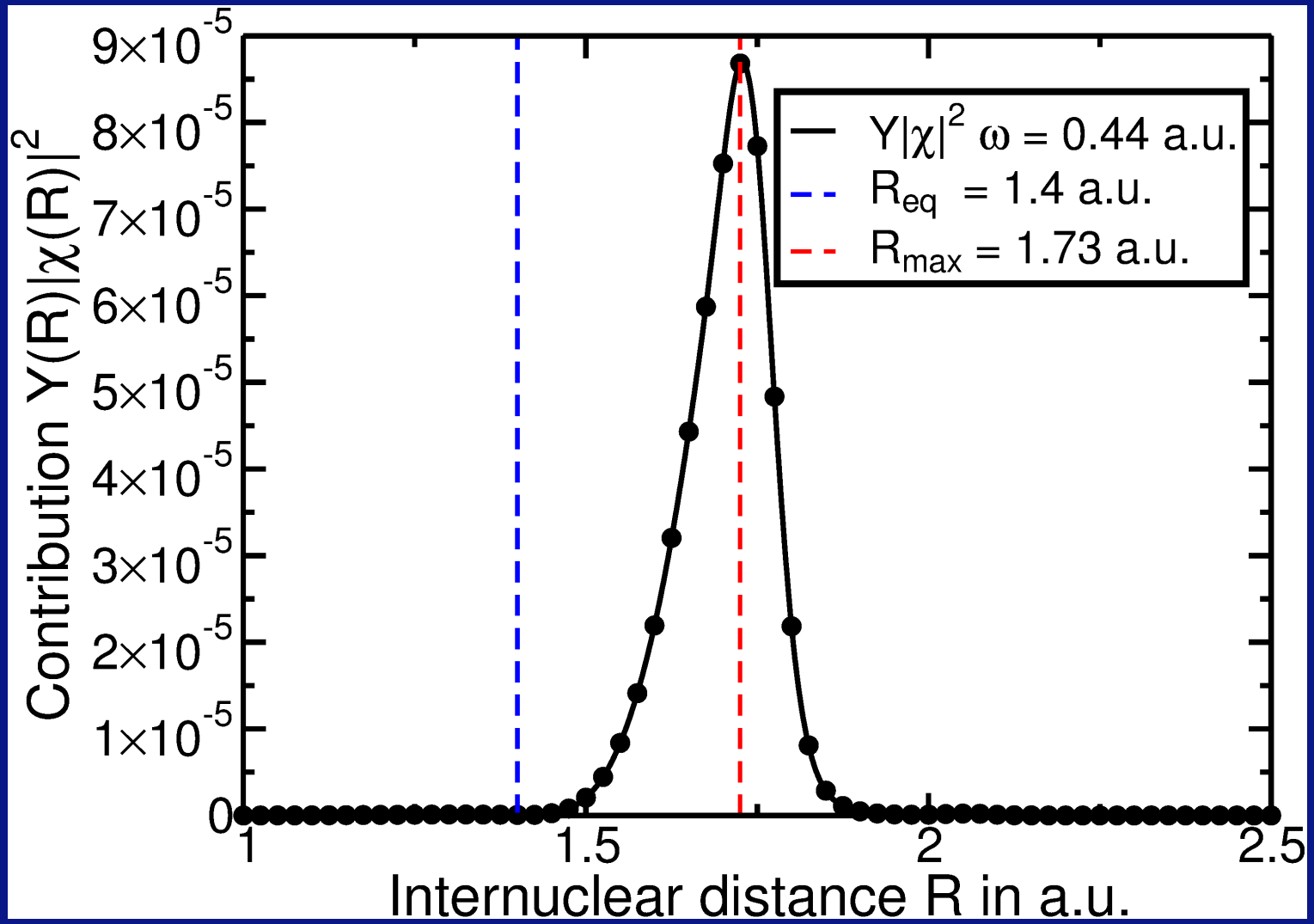

Contributions $Y(R)|\chi(R)|^2$. Pulse parameters: duration $T = 10$ fs ($\cos^2$-envelope), peak intensity $I = 10^{12}$ W cm^{-2}, alignment: $\|$.

H_2: low-intensity, high frequency regime

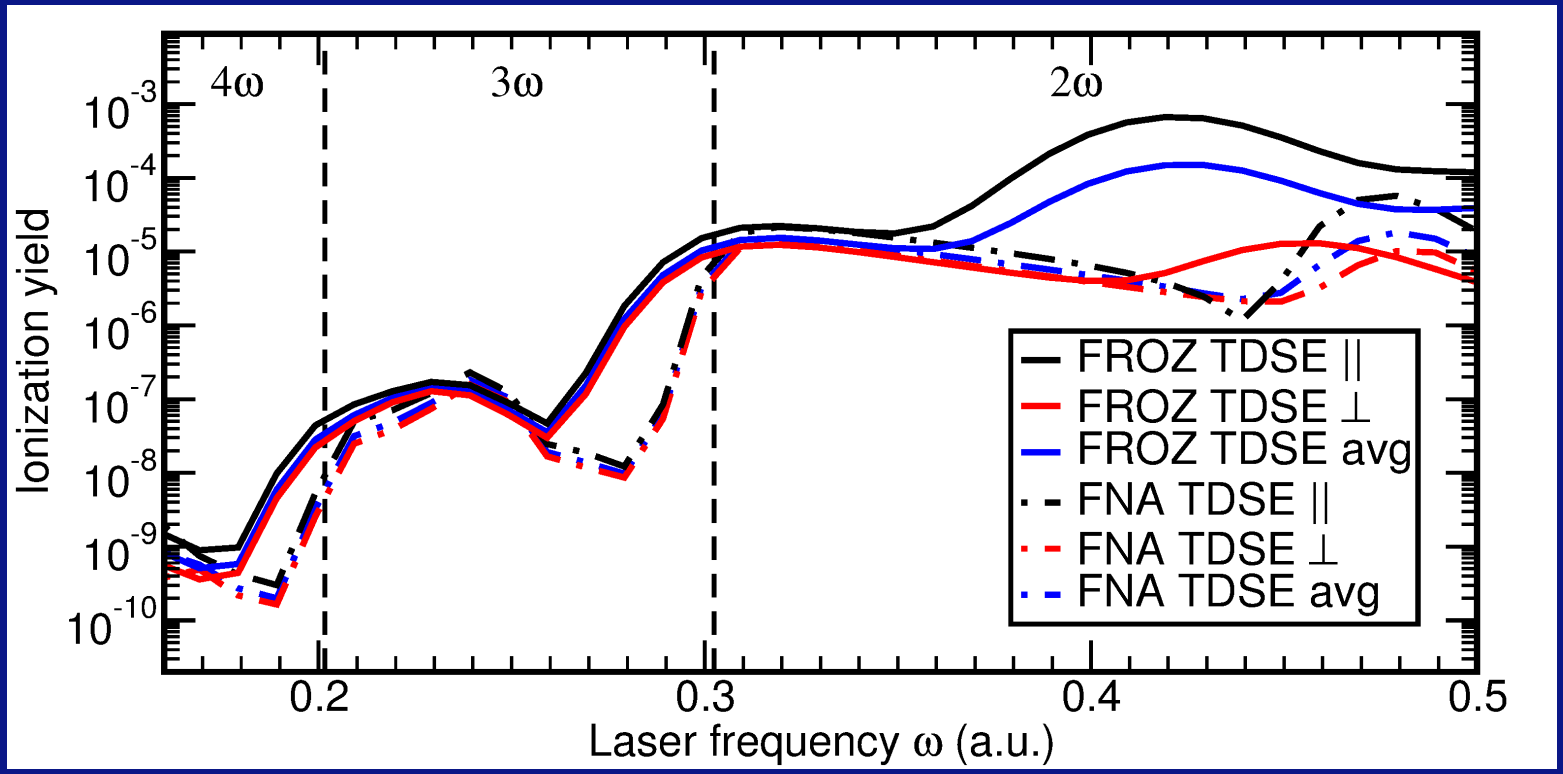

Ionization probability (frequency scan). Pulse parameters: duration $T = 10$ fs ($\cos^2$-envelope), peak intensity $I = 10^{12}$ W cm^{-2}.

$$Y_{\mathrm{avg,X}} = \int \mathrm{d}\theta \sin(\theta) Y_{\mathrm{X}}(\theta) \text{ with X = FNA or FROZ}$$

$\longrightarrow$ FNA breakdown also for randomly aligned H_2.

Summary:

- The nuclear degrees of freedom are very important!
- Many important effects may already be included when considering geometry dependent $I_P(\vec{R})$ and the frozen-nuclei approximation (FROZ)

  (should be especially true for very short pulses).
- Nuclear wavepackets in (neutral) initial electronic state may be imaged using *Lochfraß*.
- Nuclear wavepackets of the formed ion (more accurately the autocorrelation function) can be imaged by PACER.
- A PACER experiment without separately initiated dynamics may be substituted by simple time-unresolved photoelectron spectroscopy.